

# UNCLASSIFIED

AD NUMBER
AD280149
NEW LIMITATION CHANGE
TO Approved for public release, distribution unlimited
FROM Distribution authorized to U.S. Gov't. agencies and their contractors; Foreign Government Information; DEC 1961. Other requests shall be referred to British Embassy, 3100 Massachusetts Avenue, NW, Washington, DC 20008.
AUTHORITY
DSTL, DSIR 23/29561, 10 Dec 2008

THIS PAGE IS UNCLASSIFIED

**UNCLASSIFIED**

---

**AD 280 149**

*Reproduced  
by the*

**ARMED SERVICES TECHNICAL INFORMATION AGENCY  
ARLINGTON HALL STATION  
ARLINGTON 12, VIRGINIA**



---

**UNCLASSIFIED**

NOTICE: When government or other drawings, specifications or other data are used for any purpose other than in connection with a definitely related government procurement operation, the U. S. Government thereby incurs no responsibility, nor any obligation whatsoever; and the fact that the Government may have formulated, furnished, or in any way supplied the said drawings, specifications, or other data is not to be regarded by implication or otherwise as in any manner licensing the holder or any other person or corporation, or conveying any rights or permission to manufacture, use or sell any patented invention that may in any way be related thereto.

280149

TECH. NOTE  
AERO. 2803

2843  
TECH. NOTE  
AERO. 2803

7

**ROYAL AIRCRAFT ESTABLISHMENT**  
(BEDFORD)

TECHNICAL NOTE No. AERO. 2803

AD No. \_\_\_\_\_  
ASTIA FILE COPY

**FURTHER EXPERIMENTAL INVESTIGATIONS  
OF THE CHARACTERISTICS OF CAMBERED  
GOTHIC WINGS AT MACH NUMBERS  
FROM 0.4 TO 2.0**

by

L. C. Squire, Ph.D.

280149

ASTIA  
RECEIVED  
APR 30 1962  
RESERVED  
TISIA D

DECEMBER, 1961

THE RECIPIENT IS WARNED THAT INFORMATION  
CONTAINED IN THIS DOCUMENT MAY BE SUBJECT  
TO PRIVATELY-OWNED RIGHTS.

MINISTRY OF AVIATION, LONDON, W.C.2.

UNCLASSIFIED

U.D.C. No. 533.693.3 : 533.6.032 : 533.6.013.1 : 533.6.011.34/5

Technical Note No. Aero 2803

December, 1961

ROYAL AIRCRAFT ESTABLISHMENT

(BEDFORD)

FURTHER EXPERIMENTAL INVESTIGATIONS OF THE CHARACTERISTICS  
OF CAMBERED GOTHIC WINGS AT MACH NUMBERS FROM 0.4 TO 2.0

by

L. C. Squire, Ph.D.

---

SUMMARY

The wind tunnel tests on cambered gothic wings reported in Reports and Memoranda No.3211 have been extended to include the effects of changes in design lift coefficient and of changes in spanwise camber without changes in camber incidence distribution.

It was found that the camber was successful in that the flow was attached over the whole wing at the design lift. Also at the design lift the lift-dependent drag was close to the predicted values. However, the lift-dependent drag of the uncambered wing was also close to this value so that the benefit of camber on lift/drag ratio was very small. At subsonic speeds the cambered wings were less stable than the uncambered wing; also the changes of stability with incidence and Mach number were greater, particularly near  $M = 1.0$ .

Changes in spanwise camber, without changes in incidence distribution, do not alter the force characteristics near the design lift, but do alter the off-design characteristics.

---

UNCLASSIFIED

LIST OF CONTENTS

	<u>Page</u>
1 INTRODUCTION	4
2 DETAILS OF TESTS	4
2.1 Description of models	4
2.2 Range of tests	5
2.3 Accuracy of results	6
3 PRESENTATION AND DISCUSSION OF RESULTS	6
3.1 Flow and force development on wings 1 and 3 at supersonic speeds	7
3.2 Effects of camber design lift coefficient	8
3.2.1 Lift and pitching moment	8
3.2.2 Drag	9
3.3 Effect of change in wing shape	10
3.4 Low speed, high incidence, results for wings 3 and 4	10
4 CONCLUSIONS	11
LIST OF SYMBOLS	12
LIST OF REFERENCES	12
ADVANCE DISTRIBUTION LIST	13
TABLE 1 - Details of models	14
ILLUSTRATIONS - Figs.1-34	-
DETACHABLE ABSTRACT CARDS	-

LIST OF ILLUSTRATIONS

	<u>Fig.</u>
Details of plane wing (wing 1)	1
Details of camber design	2
Details of wing cross-sections: wings 1, 2 and 3	3
Details of wing cross-sections: wings 3 and 4	4
Variation of $C_L$ with $\alpha$ : wings 1 and 3	5
Variation of $C_m$ with $C_L$ : wings 1 and 3	6
Variation of $C_D$ with $C_L$ : wings 1 and 3	7
Variation of $L/D$ with $C_L$ : wings 1 and 3	8

LIST OF ILLUSTRATIONS (CONTD)

	<u>Fig.</u>
Oil flow photographs: wing 3: $M = 1.61$	9(a)&(b)
Oil flow photographs: wing 3: $M = 2.0$	10
Oil flow photographs: wing 1	11(a)&(b)
Variation of $C_L$ with $\alpha$ : wing 1	12
Variation of $C_m$ with $C_L$ : wing 1	13
Variation of $C_D$ with $C_L$ : wing 1	14
Variation of $C_L$ with $\alpha$ : wing 2	15
Variation of $C_m$ with $C_L$ : wing 2	16
Variation of $C_D$ with $C_L$ : wing 2	17
Variation of $C_L$ with $\alpha$ : wing 3	18
Variation of $C_m$ with $C_L$ : wing 3	19
Variation of $C_D$ with $C_L$ : wing 3	20
Variation of $(C_L - \bar{C}_L)$ with $(\alpha - \bar{\alpha})$ : wings 1, 2 and 3	21
Variation of $(C_m - \bar{C}_m)$ with $(C_L - \bar{C}_L)$ : wings 1, 2 and 3	22
Variation of centre of pressure position with $C_L$ at constant Mach number: wings 1, 2 and 3	23
Variation of centre of pressure position with Mach number at fixed $C_L$ : wings 1, 2 and 3	24
Comparison of drag polars of wings 1, 2 and 3	25
Variation with Mach number of the drag at fixed $C_L$ : wings 1, 2 and 3	26
Variation with $C_L$ of the lift-dependent drag factor: wings 1, 2 and 3	27
Comparison of the zero lift drag of wing 1 with theory	28
Variation of $C_L$ with $\alpha$ : wings 3 and 4	29
Variation of $C_m$ with $C_L$ : wings 3 and 4	30
Variation of $C_D$ with $C_L$ : wings 3 and 4	31
Variation of $C_L$ with $\alpha$ : $M = 0.4$ : wings 3 and 4	32
Variation of $C_m$ with $C_L$ : $M = 0.4$ : wings 3 and 4	33
Variation of $C_D$ with $C_L$ : $M = 0.4$ : wings 3 and 4	34

## 1 INTRODUCTION

In connection with the design of slender wings for high lift over drag, an experimental investigation of slender wing models with curved leading edges and various types of camber is being made in the 3 ft tunnel at R.A.E., Bedford. The results of tests at supersonic speeds on the first two wings in this programme were presented in Ref.1. Both of these wings were of gothic planform, aspect ratio 0.75, with the same thickness distribution. One wing was uncambered and the other was cambered by Weber's method<sup>2</sup> to have completely attached flow and low drag-due-to-lift at the design lift coefficient  $\{(C_L)_d = 0.1\}$ . Tests, both at supersonic speeds<sup>1</sup> and at low speeds<sup>3</sup>, on this first cambered wing showed that the large droop of the wing near the leading edge retarded the development of leading edge separation at off-design conditions.

In the present Note tests at supersonic speeds on two more cambered gothic wings are described. On both these wings the amount of leading edge droop was decreased by reducing the design lift coefficient to 0.05; the two designs were obtained by integrating the camber incidence distribution with two different initial conditions (see section 2.1 for details).

The Note also includes results of tests on all four wings at subsonic and transonic speeds.

## 2 DETAILS OF TESTS

### 2.1 Description of models

All the cambered wings tested in the present programme were designed by a method described by Weber<sup>2</sup>. One feature of this design method is of particular relevance in the present programme. The camber design is based on "slender, thin wing" theory which yields, for a given load distribution, a formula for the local incidence distribution,  $\frac{\partial z}{\partial x}(x,y)$ . This incidence distribution must then be integrated with respect to  $x$  to obtain the camber surface. The integration introduces an arbitrary function of  $y$  (the spanwise co-ordinate), this function Weber fixed by making the wing trailing edge straight, i.e. by putting  $z = \text{constant}$  at  $x = c_o$ . For structural and aerodynamic reasons it may be desirable to modify this condition, and the fourth wing in the present series is designed to find the effect of a change in this function of  $y$  (see Fig.4 and below).

Full details of the four wings are given in Table 1 and in Figs.1 to 4, where the wings are designated by the numbers 1 to 4. Wing 1 is the uncambered wing and wing 2 the cambered wing of Ref.1. Wing 3 has the same type of camber incidence distribution as wing 2, but the amount of camber (and hence of leading edge droop) has been decreased by reducing the design  $C_L$  to 0.05. Wing 4 has the same camber incidence distribution as wing 3, but differs in actual shape as the camber surface was obtained by making the wing straight (i.e.  $z = \text{constant}$ ) at  $x = 0.8 c_o$  instead of at  $x = c_o$  as on wing 3.

Wing 1 was made of steel throughout, but the three cambered wings were made of glasscloth and araldite formed onto a metal core. In all models a small circular body of 1.35 inches diameter was used at the rear of the model to shield the balance and sting support (Fig.1).



## 2.2 Range of tests

The tests were made in the transonic and supersonic test sections of the 3 ft tunnel at R.A.E., Bedford. The range of force tests, consisting of measurements of lift, drag and pitching moment, is given in the following table:

Wings	Test Section	Mach numbers	Incidence Range (1° steps)
3	Supersonic	1.42, 1.61, 1.82, 2.0	-5° to +12°
4	Supersonic	1.42, 1.61, 1.82, 2.0	-5° to +10°
1 and 2	Transonic	0.4, 0.7, 0.8, 0.85, 0.9, 0.94, 0.98, 1.02, 1.25, 1.30	-5° to +10°
3	Transonic	0.4, 0.7, 0.9, 0.94, 0.98, 1.02, 1.25, 1.30	-2° to +13°
4	Transonic	0.4, 0.7, 0.9, 0.94, 0.98	-2° to +10°
3 and 4	Nominal supersonic test section with unshaped (flat) wall	0.4	-2° to +17°

All tests were made at a Reynolds number of  $2 \times 10^6$  based on aerodynamic mean chord.

The force tests on wings 1 and 2 at supersonic speeds<sup>1</sup> with free transition showed that extensive regions of laminar flow occurred on the wings at low incidence. It was also found that turbulent flow over the whole wing could be obtained with bands of carborundum along the leading edge; these bands of carborundum did not change the lift or pitching moment, but did increase the drag. For all the present force tests therefore, transition was fixed with bands of carborundum along the full length of the leading edge; the bands were approximately 0.5" wide normal to the leading edge and started 0.125" inboard of the edge. Two grades of carborundum were used, the grain size being 0.007" for  $M = 1.42$  and above and 0.003" for lower speeds. Oil-flow tests suggested that these bands had in fact fixed transition throughout the incidence range at all Mach numbers.

During initial tests on wings 1 and 2 in the transonic test section, large fluctuating stresses occurred in the balance\*. Near  $M = 0.80$  these reached a peak value which was considered dangerous; hence no measurements were made on wings 3 and 4 between  $M = 0.70$  and  $0.90$ .

---

\*The vibrations which were responsible for these fluctuating stresses occurred when the natural frequency of the model system (i.e. model, balance and sting) corresponded with a frequency of main disturbances in the tunnel air stream: they had no other aerodynamic significance.

In addition to force tests, oil flow investigations were made at various Mach numbers and incidences; details are given in the following sections. Early tests with and without roughness bands showed no significant changes in vortex position or shape. Thus, since the main region of interest in the flow development occurs near the leading edge, the main oil flow tests were made without roughness bands.

### 2.3 Reduction and accuracy of results

Force results have been reduced to the usual coefficient form; on all four wings the reference areas and chords are based on the common planform. Pitching moment coefficients are given about the quarter chord point of the mean aerodynamic chord. The drag has been corrected to a base pressure on the minimum body equal to free stream static pressure.

No corrections have been applied for wind tunnel interference or for angularity of the tunnel flow. The former correction is zero at Mach numbers above  $M = 1.3$  since the reflection of the bow wave strikes the model support well downstream of the model base. Below this Mach number the interference effects are probably small, except near  $M = 1.0$ , where the measured speed may have been somewhat in error. Also, at  $M = 1.25$  and  $1.30$  measurements of base pressure suggested that flow at the model base was still affected by wall interference. Hence the drag results at these Mach numbers were considered not reliable and have not been presented.

Apart from tunnel interference it is estimated that the accuracy of the results is as follows:

$$\begin{aligned} C_L &\pm 0.003 \\ C_m &\pm 0.0005 \\ \left. \begin{aligned} C_D &\pm 0.0004 \text{ at } C_L = 0 \\ &\pm 0.001 \text{ at } C_L = 0.3 \end{aligned} \right\} M > 1.42 \\ \alpha &\pm 0.05^\circ \text{ from measurement, together} \\ &\text{with a possible error of } \pm 0.1^\circ \text{ from} \\ &\text{flow angularity.} \end{aligned}$$

The errors in drag measurement may be slightly greater at subsonic speeds owing to the balance vibration mentioned in last section; also all the results at  $M = 0.4$  are subject to larger errors than those listed above owing to the low level of loading at this Mach number.

## 3 PRESENTATION AND DISCUSSION OF RESULTS

Full results for wings 1 and 2 at supersonic speeds are given in Ref.1. Force results for wings 3 and 4 at supersonic speeds and for all four wings at subsonic and transonic speeds are given in the present Note. Graphical presentation has been adopted (see Figs.5 to 8 and 12 to 20).

In discussing the results some cross-reference to the earlier report is obviously necessary. In order to keep this reference to a minimum the discussion has been divided into four parts. In the first part, results for wing 3 at supersonic speeds are discussed, and the behaviour of this wing is compared with that already described for wings 1 and 2 in Ref.1. The other three sections then deal with topics which are less related to the subject matter of Ref.1.

### 3.1 Flow and force development on wings 1 and 3 at supersonic speeds

The variations of  $C_L$  with  $\alpha$ , and of  $C_m$ ,  $C_D$  and  $L/D$  with  $C_L$  for wings 1 and 3 are compared in Figs.5 to 8. Oil flow photographs for wing 3 at a series of incidences at  $M = 1.61$  and  $M = 2.0$  are given in Figs.9(a), 9(b) and 10. Comparable photographs for wing 1 (though not at identical incidences) are shown in Figs.11(a) and 11(b).

Before discussing the results it should be recalled that in the investigation<sup>1</sup> of the flow development on wing 2 at supersonic speeds it was found that the flow remained attached at the leading edge, and over the whole wing, for an incidence range on both sides of the design incidence; also the lift curve slopes were linear throughout the test range. At the same Mach numbers the flow separated from the leading edge of wing 1 at very low incidence and the separated sheet rolled into a vortex which produced a non-linear lift contribution; the size of this contribution decreased with increase of Mach number.

The results plotted in Figs.5 to 8 show that apart from a displacement of the curves the force results for wing 3 are similar to those of wing 1, and again the non-linearity of the lift and moment curves decreases with increase in Mach number.

The oil flow photographs (Figs.9(a) and 9(b)) at  $M = 1.61$  for wing 3 show that separations do occur on this wing at small incidences away from the design point ( $C_L = 0.05$ ), but there is still a small incidence range in which the flow is attached, for example at  $\alpha = 3.1^\circ$  ( $C_L = 0.070$ ) and  $\alpha = 2.0^\circ$  ( $C_L = 0.045$ ) the flow was attached on both surfaces of the wing\*. (The actual flow patterns at  $\alpha = 2^\circ$  are almost identical to those at  $\alpha = 3.1^\circ$  and so are not presented.) Above these incidences the lower surface oil pattern remains similar to that at  $\alpha = 3.1^\circ$  but a separation occurs on the upper surface. The vortex associated with this separation is quite small but can be seen in the photograph for  $\alpha = 4.2^\circ$  ( $C_L = 0.097$ ) over the outer half of the leading edge where the attachment and secondary separation lines are clearly visible<sup>4</sup>. At higher incidences ( $\alpha = 6.3^\circ$  and  $8.4^\circ$ ) separation starts nearer the apex and the attachment and secondary separation lines move inboard. It should be noted that at  $\alpha = 6.3^\circ$ , i.e. approximately  $4^\circ$  above the design point, the shape and position of the vortex is similar to that on the plane wing at  $\alpha = 4^\circ$  (Fig.11(b)). At incidences below  $\alpha = 2^\circ$  separation occurs along most of the leading edge, and a vortex lies along the lower surface (see photograph for  $\alpha = 0$ ).

At  $M = 2.0$  the photographs (Fig.10) of oil flow do not show a single large vortex, even at  $\alpha = 8^\circ$ ; instead at this incidence the oil flow could be interpreted as showing a series of small vortices running back over the wing. However, the lift curve slope for this Mach number begins

---

\*In the interpretation of these photographs it should be noted that the regions of unmoved oil which exist at most incidences represent regions of attached laminar flow. For example on the lower surface at  $\alpha = 3.1^\circ$  the oil has formed streamlines near the leading edge due to the high shear in the laminar attached flow there. Further inboard the oil is unmoved except for two regions at the rear of the wing where the well defined oil lines indicate that transition has occurred. It should be noted that roughness which was used to fix transition in the force tests was removed for the visualisation tests in order to obtain details of the flow in the immediate vicinity of the edge. Thus the transition changes do not occur in the force tests.

to increase at incidences above about  $6^\circ$  incidence, the rate of increase being less than at lower Mach numbers. Thus it would appear that although a single vortex has not formed at  $8^\circ$  incidence, a change in the flow has nevertheless taken place which causes an increase in lift curve slope.

On wing 1 there appears to be little change in the surface flow pattern as the Mach number is increased from 1.6 to 2.0; the only change being that the vortex starts nearer the wing apex at the lower Mach number. Thus the decrease in non-linear lift on this wing with increase in Mach number is probably associated with changes in the vortex strength, which might not produce large changes in the surface flow pattern, rather than with the disappearance of the vortex as on wing 3.

### 3.2 Effects of camber design lift coefficient

#### 3.2.1 Lift and pitching moment

The variation of  $C_L$  with  $\alpha$  and of  $C_m$  with  $C_L$  for wings 1 and 3 are compared in Figs. 5 and 6 for Mach numbers between  $M = 1.42$  and  $M = 2.0$ . Similar curves for wings 1, 2 and 3 between  $M = 0.4$  and  $M = 1.3$  are given in Figs. 12 and 13, 15 and 16 and 18 and 19.

These figures show that in addition to giving a positive no-lift angle and a non-zero pitching moment at zero lift, camber also causes a displacement to higher lift coefficient of the minimum slope of the lift and moment curves. This minimum slope occurs at, or near, the condition of flow attachment and the non-linear behaviour of the curves away from this condition is associated with the growth of leading edge separations. In order to study this non-linearity in more detail results at Mach numbers of 0.7, 0.9, 1.02, 1.61 and 2.0 have been replotted in the form of  $(C_L - \bar{C}_L)$  against  $(\alpha - \bar{\alpha})$  and  $(C_m - \bar{C}_m)$  against  $(C_L - \bar{C}_L)$  {Figs. 21 and 22}, where  $\bar{\alpha}$ ,  $\bar{C}_L$  and  $\bar{C}_m$  are values of  $\alpha$ ,  $C_L$  and  $C_m$  corresponding to the minimum lift curve slope.

Fig. 21 shows that the lift development about  $\bar{\alpha}$  is similar for all three wings although there are some small differences between the wings. For example, at supersonic speeds the lift curve slope of wing 2 at  $\alpha = \bar{\alpha}$  is larger than that of the other wings, also the lift of wing 2 is linear throughout the test range, and at the highest values of  $(\alpha - \bar{\alpha})$  wing 3 has the greatest lift. Fig. 21 also includes linear lift curve slopes as given by slender wing theory ( $C_L = \pi/2 A\alpha$ ) and, at supersonic speeds, by not-so-slender wing theory<sup>5,6</sup>. Also included are curves of  $C_L = \pi/2 A\alpha + 4\alpha^2$ ;  $4\alpha^2$  being the non-linear lift increment derived by Smith<sup>7</sup>. At  $M = 0.7$ ,  $C_L = \pi/2 A\alpha + 4\alpha^2$  slightly overestimates the total lift of wing 1 whereas at  $M = 1.02$  it provides a slight underestimate. However, at  $M = 1.02$  the initial lift curve slope is higher than  $\pi/2 A\alpha$  so that  $4\alpha^2$  is still a fair approximation to the non-linear lift increment. At  $M = 1.6$  the lift is again in fair agreement with Smith's estimate, however a study of the curves shows that this agreement is fortuitous since the initial lift curve slope is much greater than  $\pi/2 A$ , and is in fact in excellent agreement with the not-so-slender value.

The curves of  $C_m - \bar{C}_m$  against  $C_L - \bar{C}_L$  show an almost complete collapse at supersonic speeds (Fig. 22), but at subsonic and transonic speeds the range of  $C_L$  about  $\bar{C}_L$  in which the aerodynamic centre remains at a constant position before moving back increases with camber design lift coefficient.

This difference in behaviour is presumably associated with the changes in leading edge separation discussed in section 3.1. The effect of this increase in range of constant aerodynamic centre position is clearly illustrated in Figs.23 and 24, where the variations of centre of pressure position with  $C_L$  at fixed Mach number, and of centre of pressure position with Mach number for fixed  $C_L$  are compared for the three wings\*. It should be noted, however, that the large forward shift in centre of pressure position which occurs on both cambered wings near  $M = 1.0$  is associated both with a forward shift of aerodynamic centre (see Fig.22) and with a decrease in  $\bar{C}_m$  in this speed range. Reasons for the forward shift in aerodynamic centre near  $M = 1.0$  have not been found. The fact that the effect only occurs on the cambered wings rules out wind tunnel interference as the main cause, although the actual magnitude of the forward shift may be influenced by tunnel constraint effects.

### 3.2.2 Drag

Drag polars for wings 1, 2 and 3 at transonic and subsonic speeds are presented in Figs.14, 17 and 20. Similar curves for wings 1 and 3 at supersonic speeds are shown in Fig.7. All results are for wings with fixed transition. Comparative drags are plotted for fixed Mach number in Fig.25 and for fixed  $C_L$  in Fig.26.

From Fig.25 it can be seen that at negative and low positive lift coefficient, the drag of wing 1 is less than that of the cambered wings, but that with increase in  $C_L$  the drag of wing 1 becomes greater than that of the cambered wings. The drag of wing 3  $\{(C_L)_d = 0.05\}$  is always less than that of wing 2  $\{(C_L)_d = 0.10\}$ . The large increase in zero lift drag of wing 2 as compared with wings 1 and 3 is mainly due to the extensive flow separations which occur on the lower surface of wing 2 at lift coefficients below 0.10.

The drag results have also been analysed in terms of a lift dependent drag factor\*\*  $\{\pi A(C_D - C_{D_0}^i)/C_L^2\}$ . The variations of this factor with  $C_L$  for the three wings are compared in Figs.27(a) to (d) at Mach numbers of 0.4, 0.7, 0.9, 0.98, 1.42, 1.61, 1.82 and 2.0. These figures also include the theoretical values of this factor as given, at supersonic speeds, by not-so-slender theory<sup>1,5</sup>. It will be seen that the induced drag factor of wing 3 is equal to, or less than, the theoretical value, although the theoretical value only applies near  $C_L = 0.05$  where the flow is attached. The experimental factor for wing 2 is always higher than the theoretical value at the design point ( $C_L = 0.1$ ), but it drops below the design value at lift coefficients above 0.2. The differences in shape of the curves at low values of  $C_L$  for the various wings are associated with the relative positions, and shapes, of the drag polars as shown in Fig.25.

---

\*Note that, for convenience of presentation, different vertical scales are used in Figs.23 and 24.

\*\* $C_{D_0}^i$  is equal to the zero lift drag of the uncambered wing together with an increment to allow for the greater wetted areas of the cambered wings. For wing 2 the increment was 0.0006, and for wing 3, 0.0003.

In Fig.28 the zero lift drag of the plane wing is compared with theoretical estimates. The skin friction drag was calculated by a strip method<sup>1</sup> based on a flat plate turbulent boundary layer. The wave drag at supersonic speeds was calculated by slender body theory; two values are given in Fig.28 the upper corresponds to the wave drag of the wing alone, i.e. ignoring the small body at the rear of wing, while the lower curve includes the effect of this body (with zero base drag). When allowance is made for form drag it will be seen that agreement between the estimated and measured drags is good throughout the speed range.

### 3.3 Effect of change in wing shape

In this section the results on wings 3 and 4 are compared. It will be recalled that these two wings have the same local incidence distribution, but that this incidence distribution has been integrated to produce two wing shapes (see section 2.1 and Fig.4). On wing 3 the trailing edge is straight and all spanwise sections have drooped leading edges; on wing 4 spanwise sections forward of 0.8 of the root chord have drooped edges, but aft of this point the tips turn up.

The variations of  $C_L$  with  $\alpha$ ,  $C_m$  with  $C_L$  and  $C_D$  with  $C_L$  for the two wings are presented in Figs.29, 30 and 31. Figs.29 and 30 show that near the design condition ( $C_L = 0.05$ ), where the flow is attached, the lift and pitching moments of the two wings are similar, although wing 4 has slightly less lift; this lower lift corresponds to an increase of about  $0.15^\circ$  in the zero lift angle of wing 4 as compared with wing 3. Away from the design point the lift develops less rapidly and the increase in stability with increase in  $C_L$  is less on wing 4 than on wing 3. Oil flow patterns on wing 4 did not, however, show any significant differences to those on wing 3 (Figs.9(a) and (b)). In spite of this, the vortex may be weaker on wing 4, or the wing shape may be less efficient in converting the low pressures associated with the vortex into lift.

The differences in the drag results are, in general, consistent with the lower non-linear lift of wing 4; that is wing 4 produces a given lift at a higher incidence than wing 3, and so has greater drag due to lift. Near the design lift coefficient the drags of the two wings are identical at supersonic speeds, but wing 4 has a slightly higher drag at subsonic speeds; it is thought that this increase in drag is due to slight differences in the transition fixing on the two wings.

These results show that large changes in wing shape, without changes in local incidence distribution, do not produce significant effects on the overall forces when the flow is attached. However, in the present case the wing with the straight trailing edge develops more non-linear lift.

### 3.4 Low speed, high incidence, results for wings 3 and 4

A comparison of the results for wings 1 and 2 at  $M = 0.4$  with Keating's low speed results<sup>3</sup> for equivalent wings gave excellent agreement. It was thus decided to dispense with low speed models of wings 3 and 4, and to extend the tests at  $M = 0.4$  on these two wings up to  $17^\circ$ . These tests could not be made in the transonic test section due to limitations on the incidence range and so they were made in the supersonic test section with a flat top wall. The results are presented in Figs.32, 33 and 34; for comparison these figures also include results from the transonic test section up to  $10^\circ$  incidence.

The purpose of these tests at high incidence were twofold. (i) To check whether any undesirable features (for example, pitch-up) occurred at these high incidences. (ii) To study the non-linear lift at high incidence, since Keating found that, for given incidence, the wing with camber designed for  $C_L = 0.1$  (wing 2) had much less lift than the plane wing.

The results show that the forces develop smoothly with increase in incidence throughout the test range. They also show a rapid increase in non-linear lift, particularly for wing 3. At  $15^\circ$  incidence the lift coefficients for wings 3 and 4 are 0.465 and 0.425 respectively; Keating's values at this incidence were 0.50 (wing 1) and 0.37 (wing 2). Thus at these high incidences wing 3 produces nearly as much lift as wing 1 because the increased strength of the non-linear lift compensates for its positive no lift angle ( $0.6^\circ$ ) and for the smaller range of incidence where there is positive non-linear lift.

#### 4 CONCLUSIONS

The tests on cambered gothic wings reported in Ref.1 have been extended to include the investigation of changes in design lift coefficient, and of changes in wing shape without changes in the local incidence distribution. The results show that:-

(1) The camber design is successful in that the flow is attached over the whole wing at the design incidence, and for a limited range on either side of it. The incidence range over which the flow is attached on the cambered wings appears to increase with increasing supersonic Mach number, whereas on the uncambered wing the flow separates from the leading edge at a small incidence for all Mach numbers.

(2) At any given incidence the cambered wings give less lift than the uncambered wing because of the positive no-lift angle and because positive non-linear lift does not commence until a higher incidence.

(3) At subsonic and transonic speeds the rate of growth of non-linear lift is similar on all wings, but at Mach numbers above  $M = 1.4$  the cambered wing with a design lift coefficient of 0.05, and a straight trailing edge, appears to develop more non-linear lift than the uncambered wing, whereas the wing with  $(C_L)_d = 0.1$  develops no non-linear lift.

(4) Camber causes a forward moment of the wing centre of pressure position at subsonic and transonic speeds; this shift is most marked near  $M = 1.0$ . At supersonic speeds the effect of camber on centre of pressure position is small.

(5) Both the camber shapes designed for  $C_L = 0.05$  have slightly lower drags than the plane wing at positive  $C_L$ , but the drag of the camber designed for  $C_L = 0.10$  is greater than that of the uncambered wing at lift coefficients below about 0.1 at subsonic speeds and 0.15 at supersonic speeds.

(6) Changes in spanwise camber, without changes in the camber incidence distribution, do not alter the force characteristics when the flow is attached, but with separated flow the wing with the straight trailing edge develops the most non-linear lift.

LIST OF SYMBOLS

A	aspect ratio
$c(y)$	local chord
$c_o$	root chord
$\bar{c}$	mean aerodynamic chord
	$= \frac{\int_{-s_T}^{s_T} c^2(y) dy}{\int_{-s_T}^{s_T} c(y) dy}$
$C_L$	lift coefficient = Lift/qS
$C_D$	drag coefficient = Drag/qS
$(C_D)_o$	drag coefficient of plane wing at zero lift
$C_m$	pitching moment coefficient = Pitching moment/qS $\bar{c}$ (referred to quarter chord point of the mean aerodynamic chord)
$\bar{C}_L, \bar{C}_m$	lift and pitching moment coefficients at minimum lift curve slope (see section 3.2.1)
M	free stream Mach number
q	free stream dynamic pressure
S	wing area
$S(x)$	cross-sectional area distribution
$s_T$	semi-span at trailing edge
$s(x)$	equation of leading edge (local semi-span)
$\alpha$	wing incidence: incidence of uncambered centre section of cambered wings
$\bar{\alpha}$	incidence at minimum lift curve slope

LIST OF REFERENCES

<u>No.</u>	<u>Author</u>	<u>Title, etc.</u>
1	Squire, L.C.	An experimental investigation at supersonic speeds of the characteristics of two gothic wings, one plane and one cambered. R.A.E. Tech. Note No. Aero 2620. R & M 3211. May 1959.
2	Weber, J.	Design of warped slender wings with the attachment line along the leading edge. R.A.E. Tech. Note No. Aero 2530. ARC 20051. September 1957.



LIST OF REFERENCES (CONTD)

<u>No.</u>	<u>Author</u>	<u>Title, etc.</u>
3	Keating, R.F.A.	Low speed wind tunnel tests on sharp edges gothic wings of aspect ratio 3/4. R.A.E. Tech. Note No. Aero 2686. ARC 22370.
4	Maskell, E.C.	Flow separations in three dimensions. R.A.E. Report No. Aero 2565. ARC 18063. November 1955.
5	Adams, Mac C. Sears, W.R.	Slender-body theory - review and extension. Jour. Aero. Sciences Vol.20. February 1953.
6	Squire, L.C.	Some applications of not-so-slender wing theory to wings with curved leading edges. R.A.E. Tech. Note No. Aero 2703. ARC 22437. July 1960.
7	Smith, J.H.B.	A theory of the separated flow from the curved leading edge of a slender wing. R.A.E. Tech. Note No. Aero 2535. R & M 3116. ARC 20010. November 1957.

ATTACHED:

Table 1  
Drg. Nos. 41847s - 41882s  
Neg. Nos. 156,210 - 156,214  
Detachable Abstract Cards

ADVANCE DISTRIBUTION LIST:

ADAR  
ADSR(A)  
TIL - 240

TABLE 1

Details of models

Dimensions (all models)

Planform	$y = s_T \frac{x}{c_o} \left( 2 - \frac{x}{c_o} \right)$
Centre-line chord ( $c_o$ )	20 inches
Span ( $2 s_T$ )	10 inches
Aerodynamic mean chord ( $\bar{c}$ )	15 inches
Area (S)	133.3 sq inches
Distance of $\frac{\bar{c}}{4}$ aft of apex	8.75 inches
Volume ( $= 0.009 c_o^3$ )	72 cu inches

Thickness distribution (without sting fairing)

Area distribution

$$S(x) = 100.8 \left( \frac{x}{c_o} \right)^2 \left( 1 - \left( \frac{x}{c_o} \right) \right) \left( 1 - \frac{3}{2} \left( \frac{x}{c_o} \right) + \left( \frac{x}{c_o} \right)^2 - \frac{1}{4} \left( \frac{x}{c_o} \right)^3 \right) \text{ sq inches.}$$

Centreline semi-thickness

$$\frac{z}{c_o} = 0.126 \left( \frac{x}{c_o} \right) \left( 1 - \frac{x}{c_o} \right) \left( 2 - 2 \left( \frac{x}{c_o} \right) + \left( \frac{x}{c_o} \right)^2 \right).$$

Camber distribution (Ref.2)

On all the cambered wings the local incidence distribution is given by

$$\begin{aligned} \frac{\partial z}{\partial x} &= C \text{ (constant) for } 0 < |\eta| \leq \eta_o(x) \\ &= C \left[ 1 - \frac{\pi(|\eta| - \eta_o)^2}{(1 + 2\eta_o^2) \cos^{-1} \eta_o - 3\eta_o \sqrt{1 - \eta_o^2}} \right] \text{ for } \eta_o(x) \leq |\eta| < 1. \end{aligned}$$

where  $\eta = y/S(x)$   $\eta_o(x) = \frac{0.8}{2 - x/c_o}$ .

The constant C is equal to 0.0956 for wing 2 and 0.0478 for wings 3 and 4.

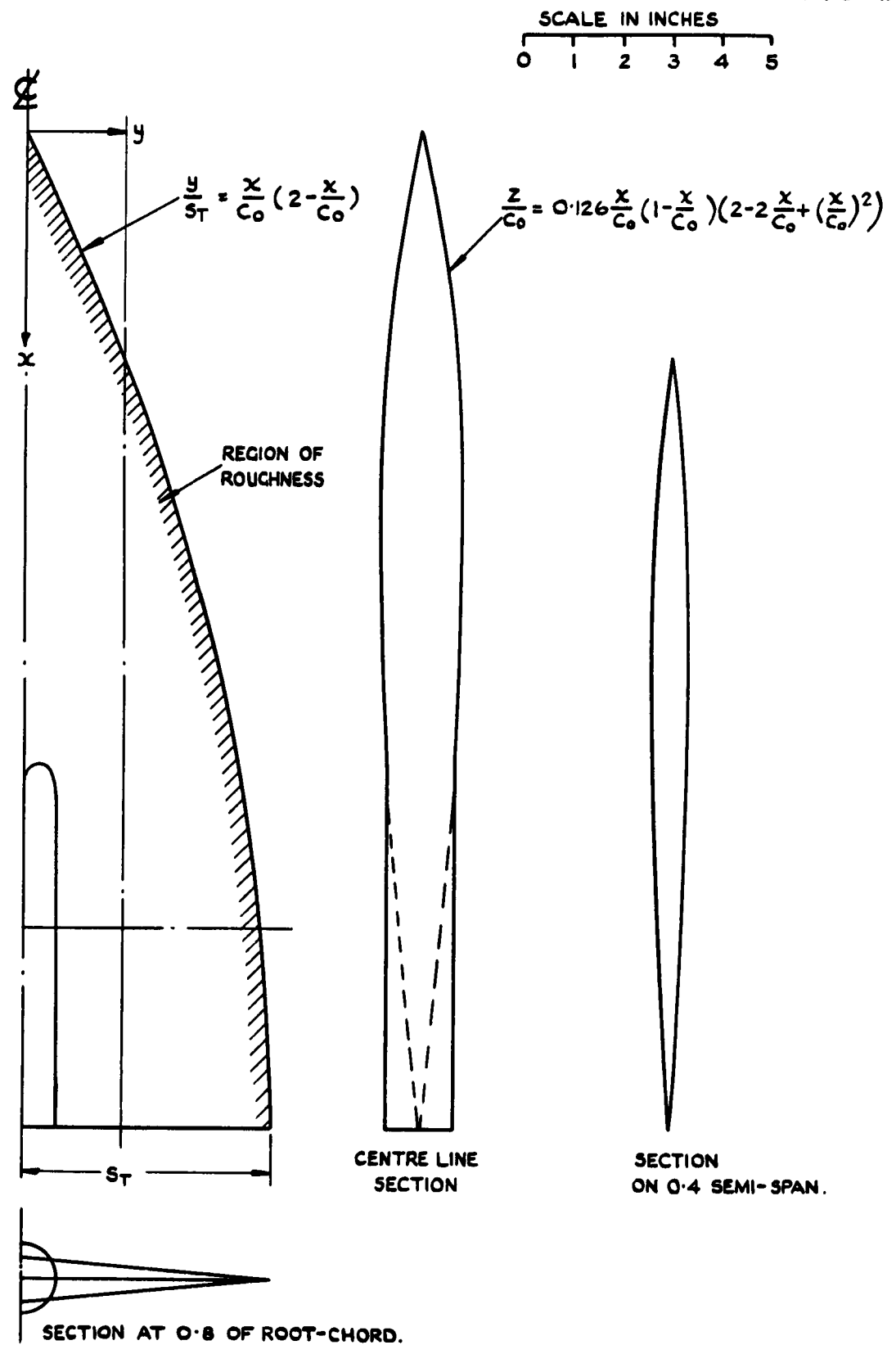


FIG. I. DETAILS OF PLANE WING (WING I)

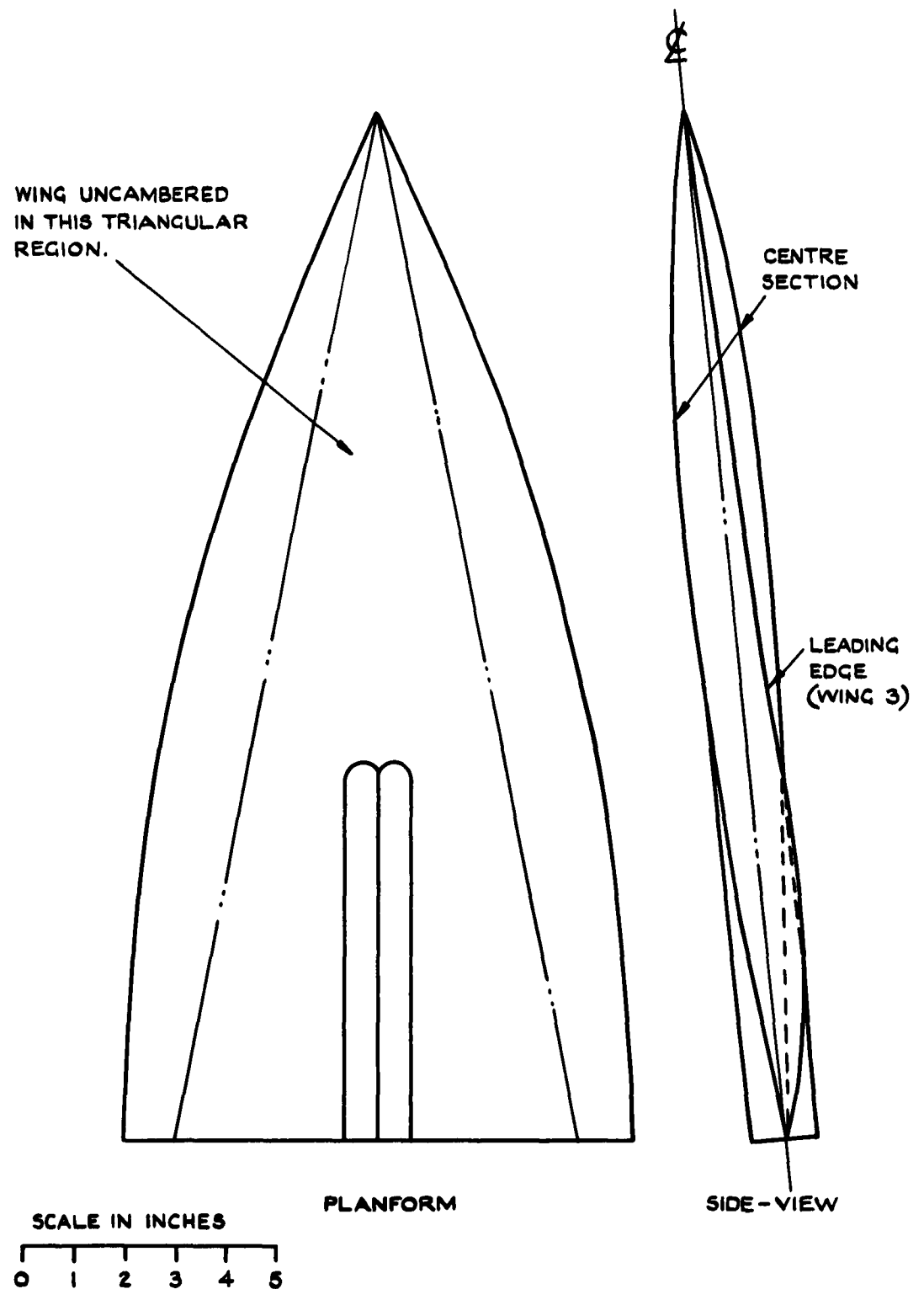


FIG. 2. DETAILS OF THE CAMBER DESIGN.

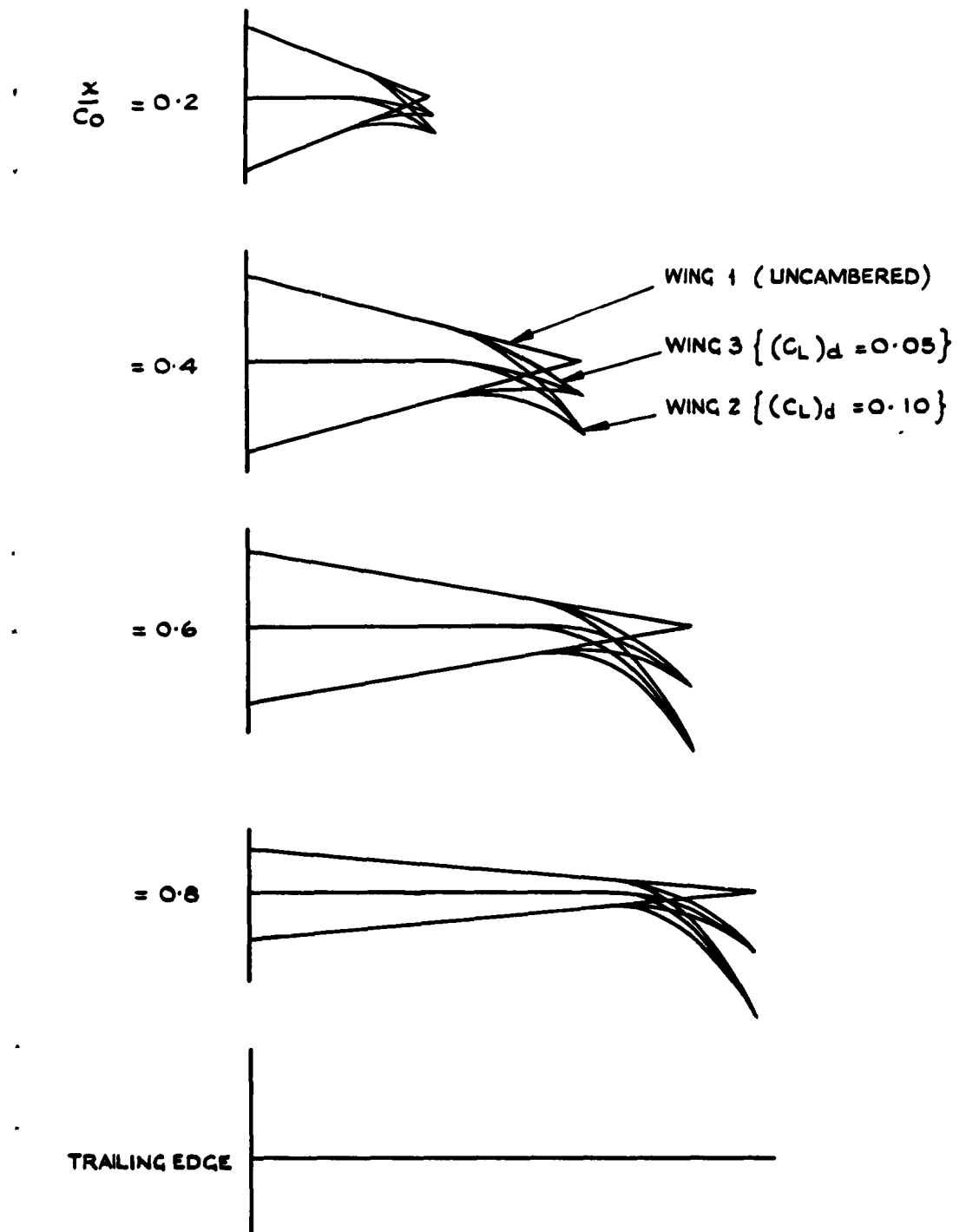


FIG. 3. DETAILS OF WING CROSS-SECTIONS  
: WINGS 1, 2 AND 3

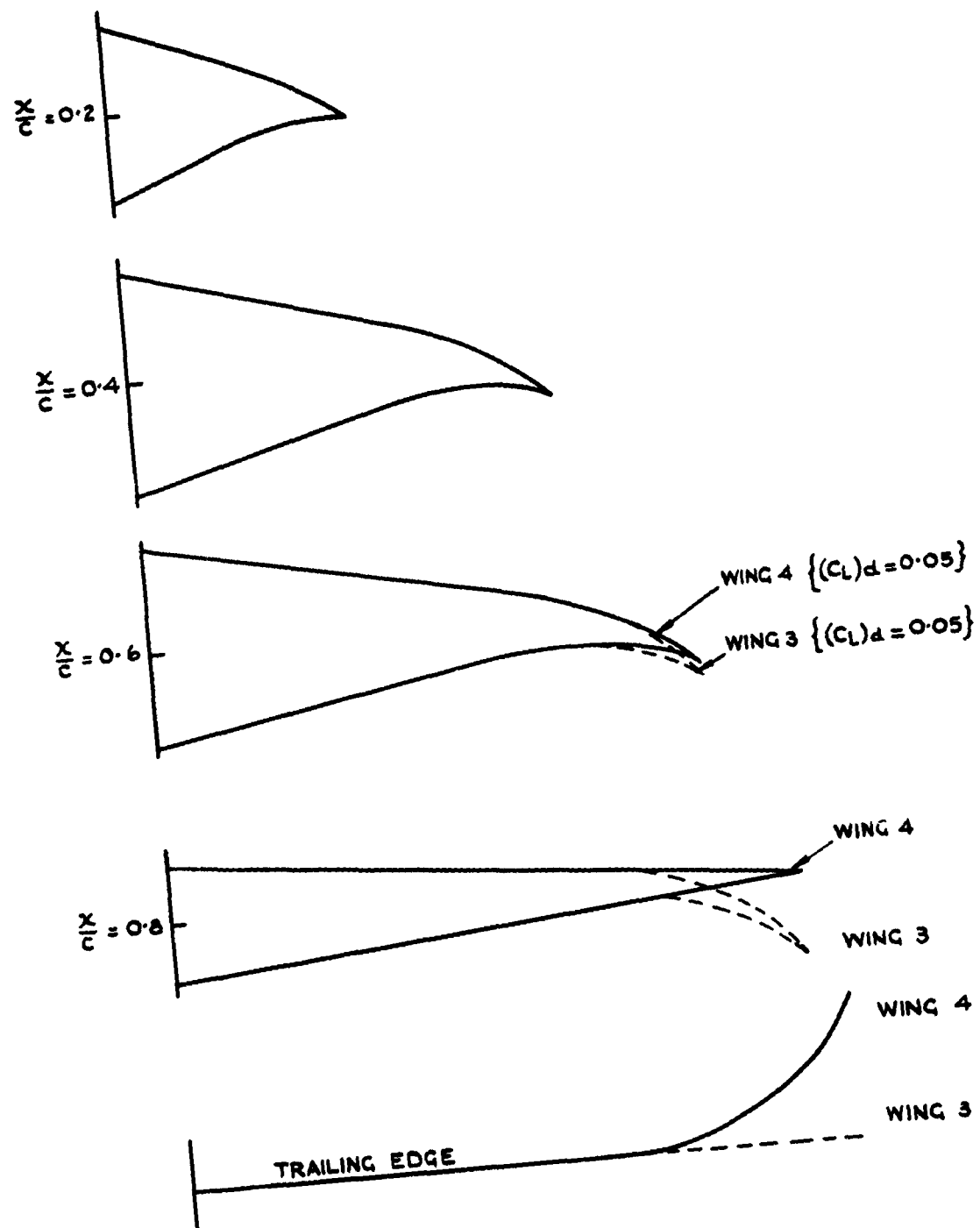


FIG. 4. DETAILS OF WING CROSS-SECTIONS:  
WINGS 3 AND 4.

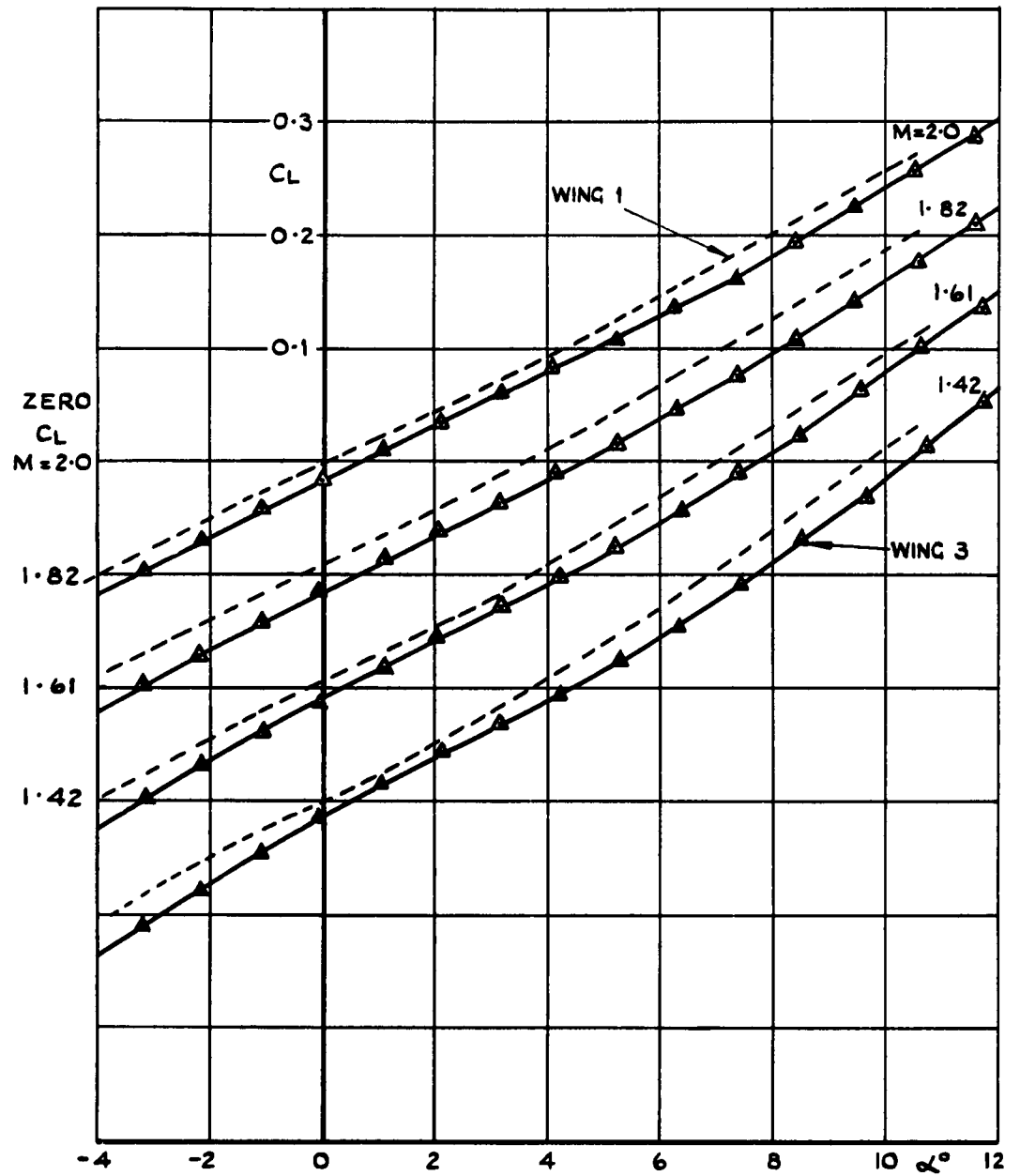


FIG. 5. VARIATION OF  $C_L$  WITH  $\alpha$ :  
WINGS 1 AND 3.

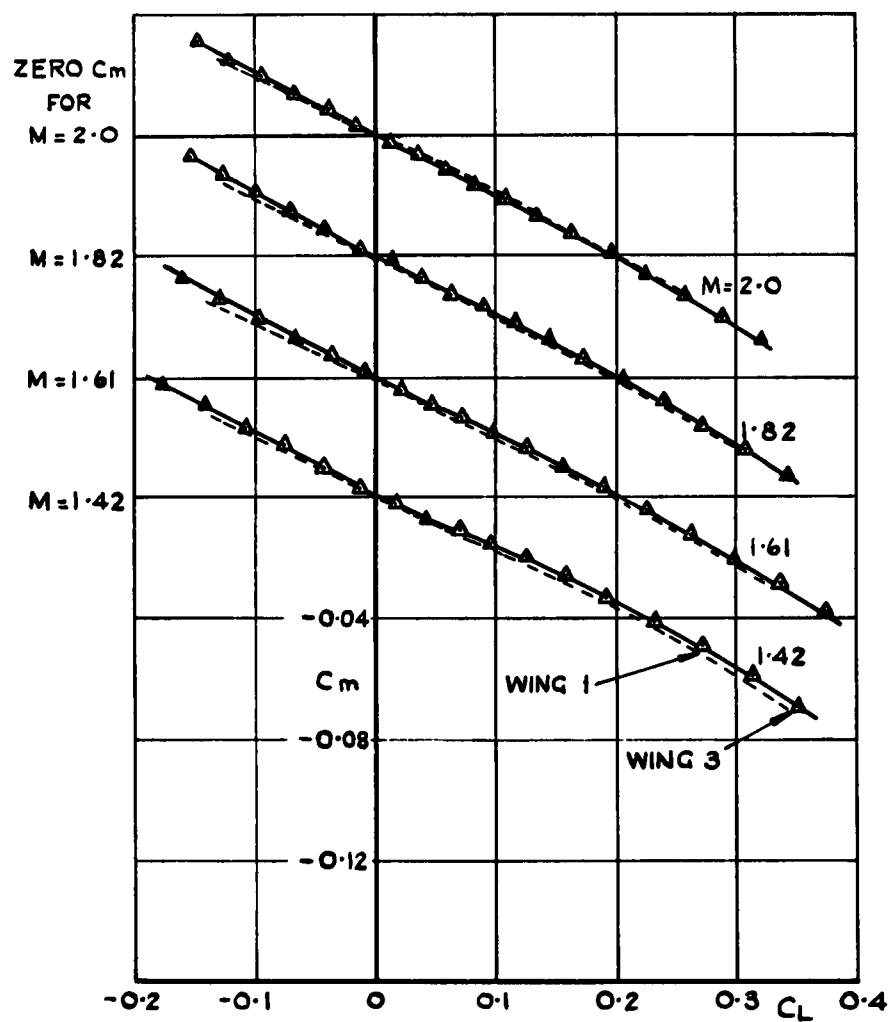


FIG. 6. VARIATION OF  $C_m$  WITH  $C_L$   
: WINGS 1 AND 3



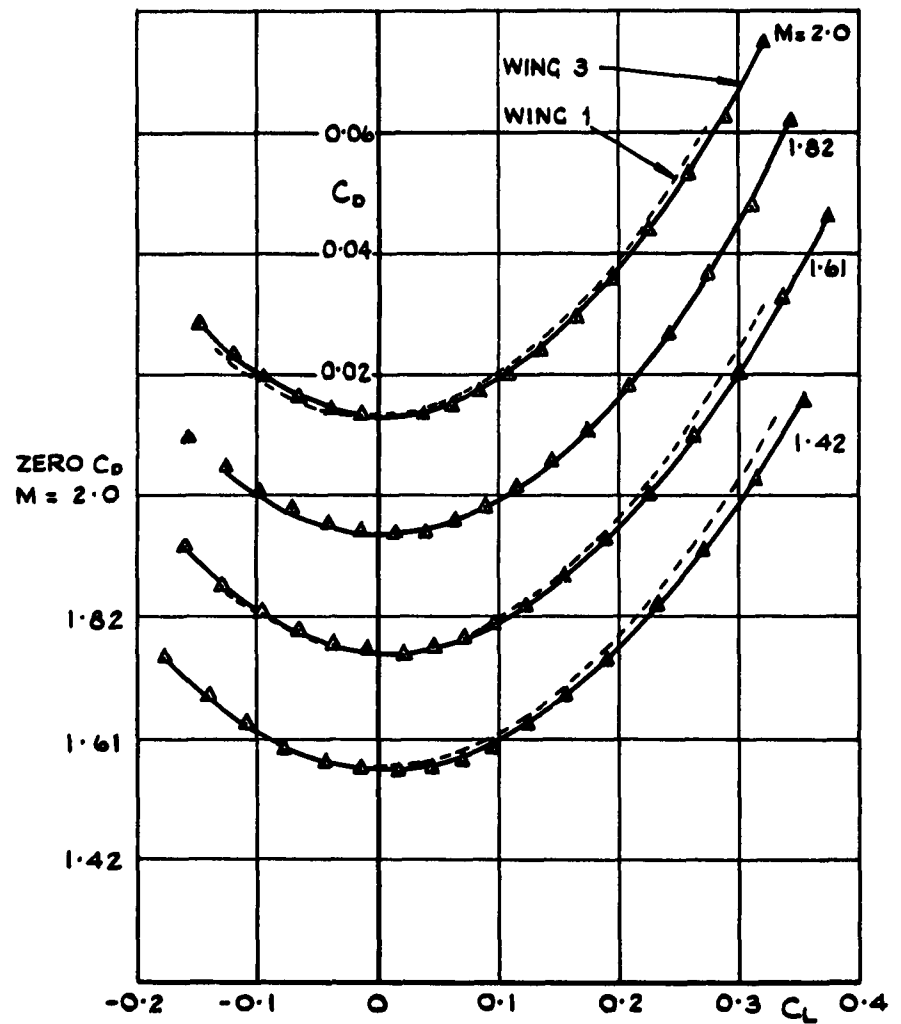


FIG. 7. VARIATION OF  $C_D$  WITH  $C_L$   
: WINGS 1 AND 3.

FIG. 8.

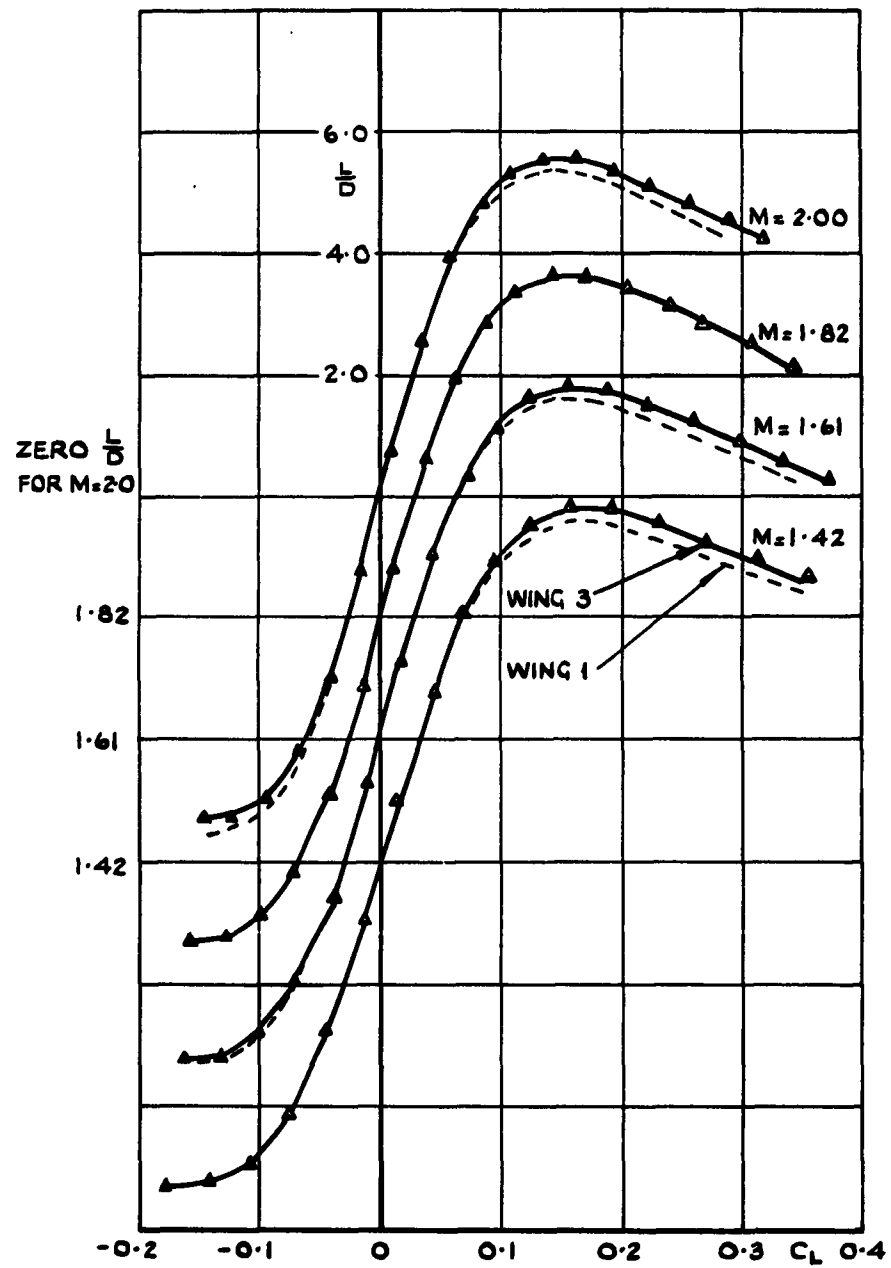
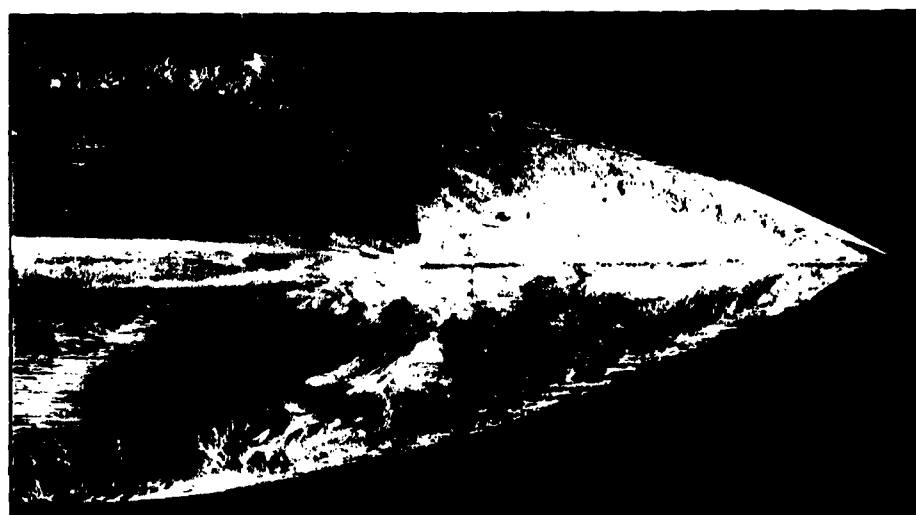


FIG. 8. VARIATION OF  $\frac{L}{D}$  WITH  $C_L$   
: WINGS 1 AND 3



$\alpha = 3.1^\circ$ : Upper surface  $C_L = 0.070$



$\alpha = 3.1^\circ$ : Lower surface  $C_L = 0.070$



$\alpha = 0$ : Lower surface  $C_L = -0.010$

FIG.9a. OIL FLOW PHOTOGRAPHS. WING 3. M 1-61



$\alpha = 8.4^\circ$ : Upper surface  $C_L = 0.223$



$\alpha = 6.3^\circ$ : Upper surface  $C_L = 0.155$

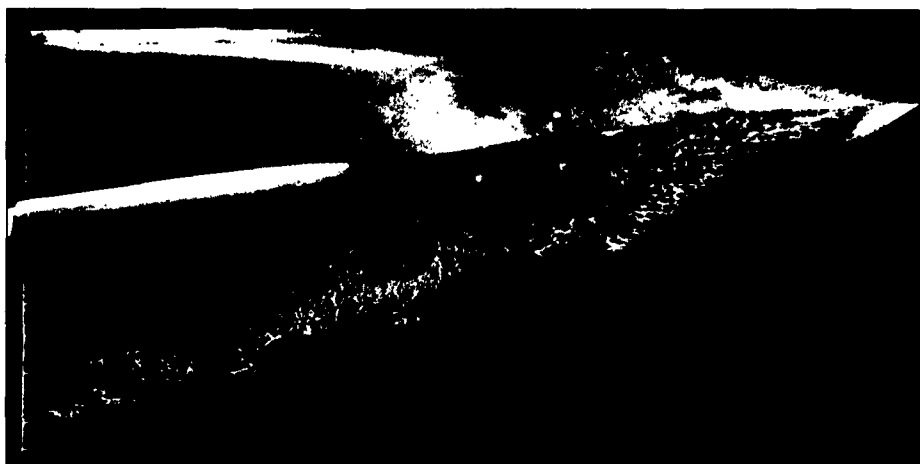


$\alpha = 4.2^\circ$ : Upper surface  $C_L = 0.097$

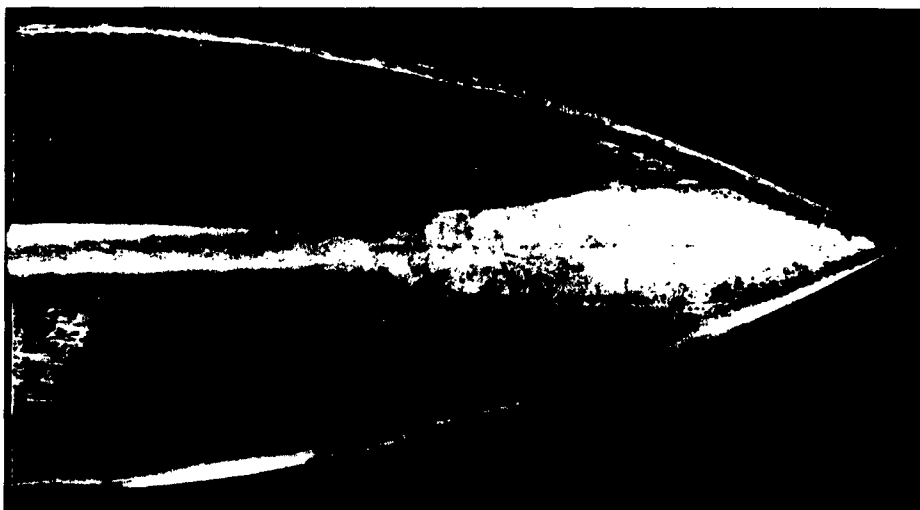
FIG.9b. OIL FLOW PHOTOGRAPHS. WING 3.  $M=1.61$



$\alpha = 8.4^\circ$ : Upper surface  $C_L = 0.193$



$\alpha = 4.2^\circ$ : Upper surface  $C_L = 0.082$



$\alpha = 0^\circ$ : Lower surface  $C_L = -0.015$

FIG.10. OIL FLOW PHOTOGRAPHS. WING 3.  $M=2.0$



$M = 1.61$



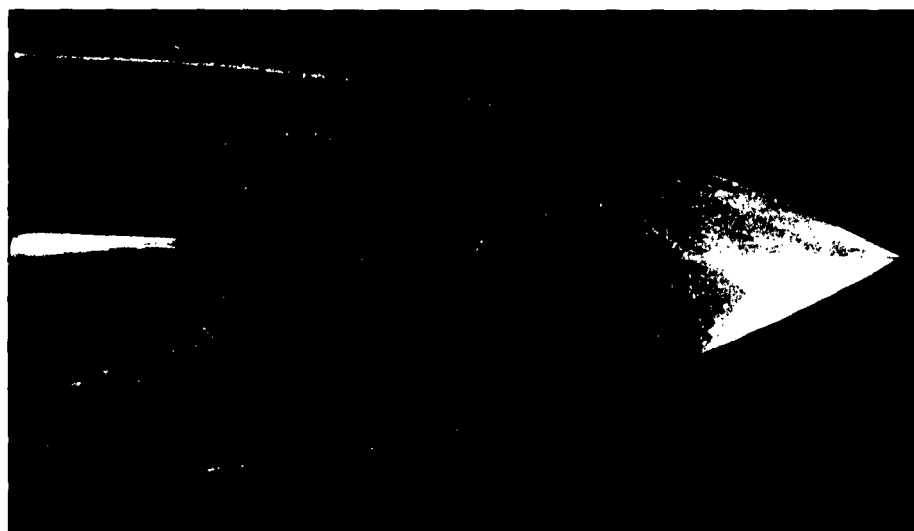
$M = 2.0$

FIG.11a. OIL FLOW PHOTOGRAPHS. WING I.

$\alpha \pm 2^\circ$



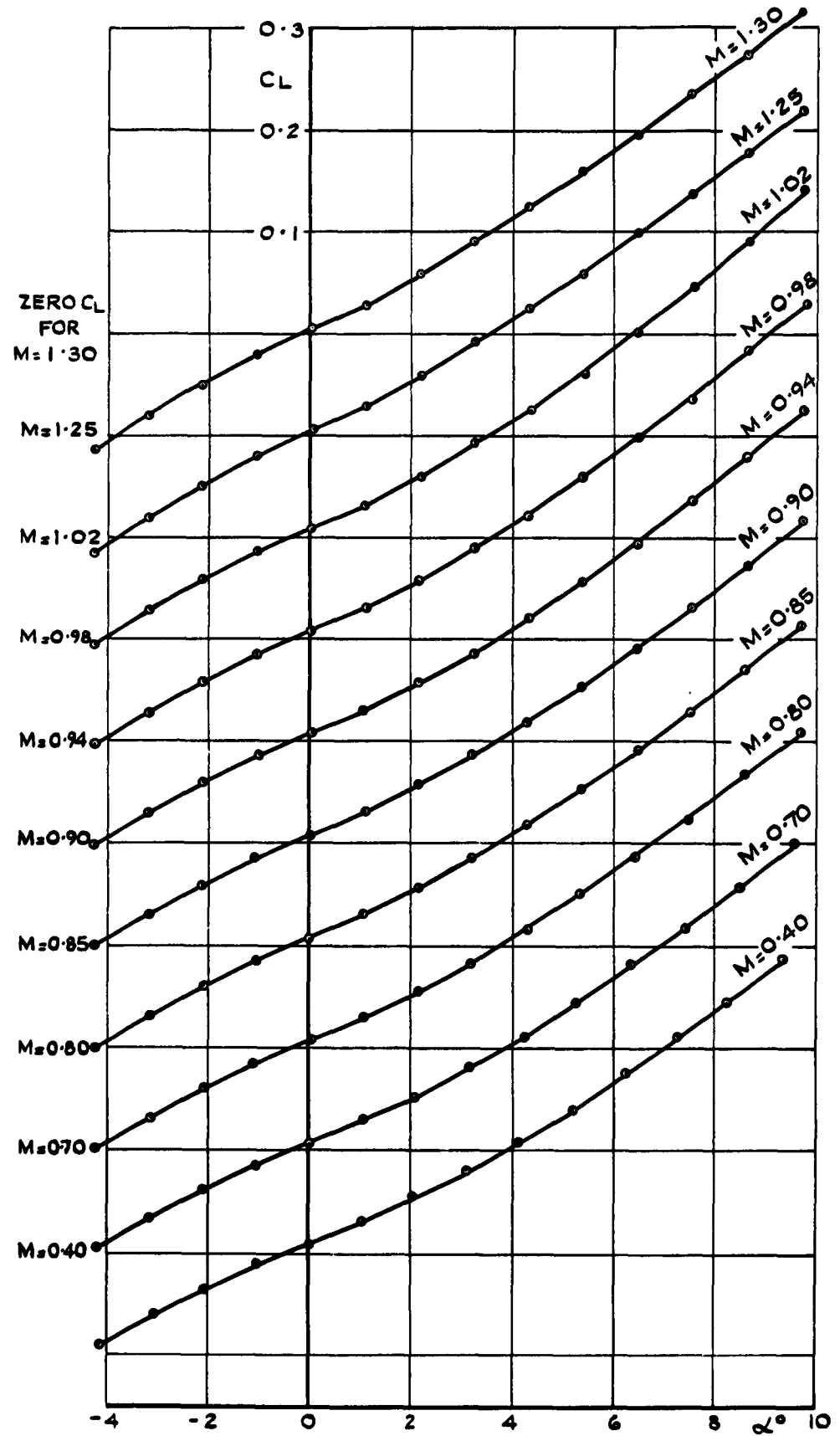
$M = 1.6$



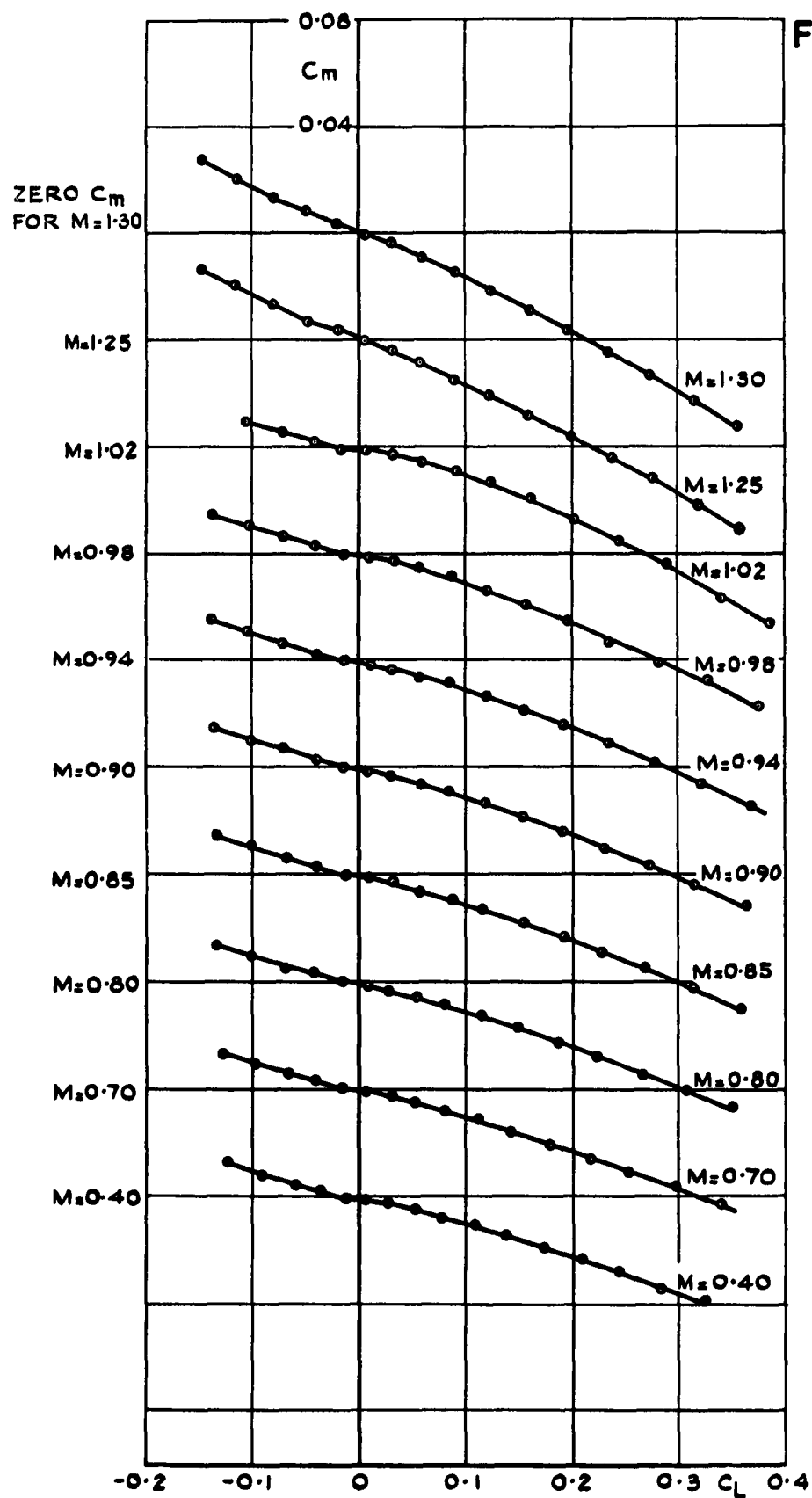
$M = 2.0$

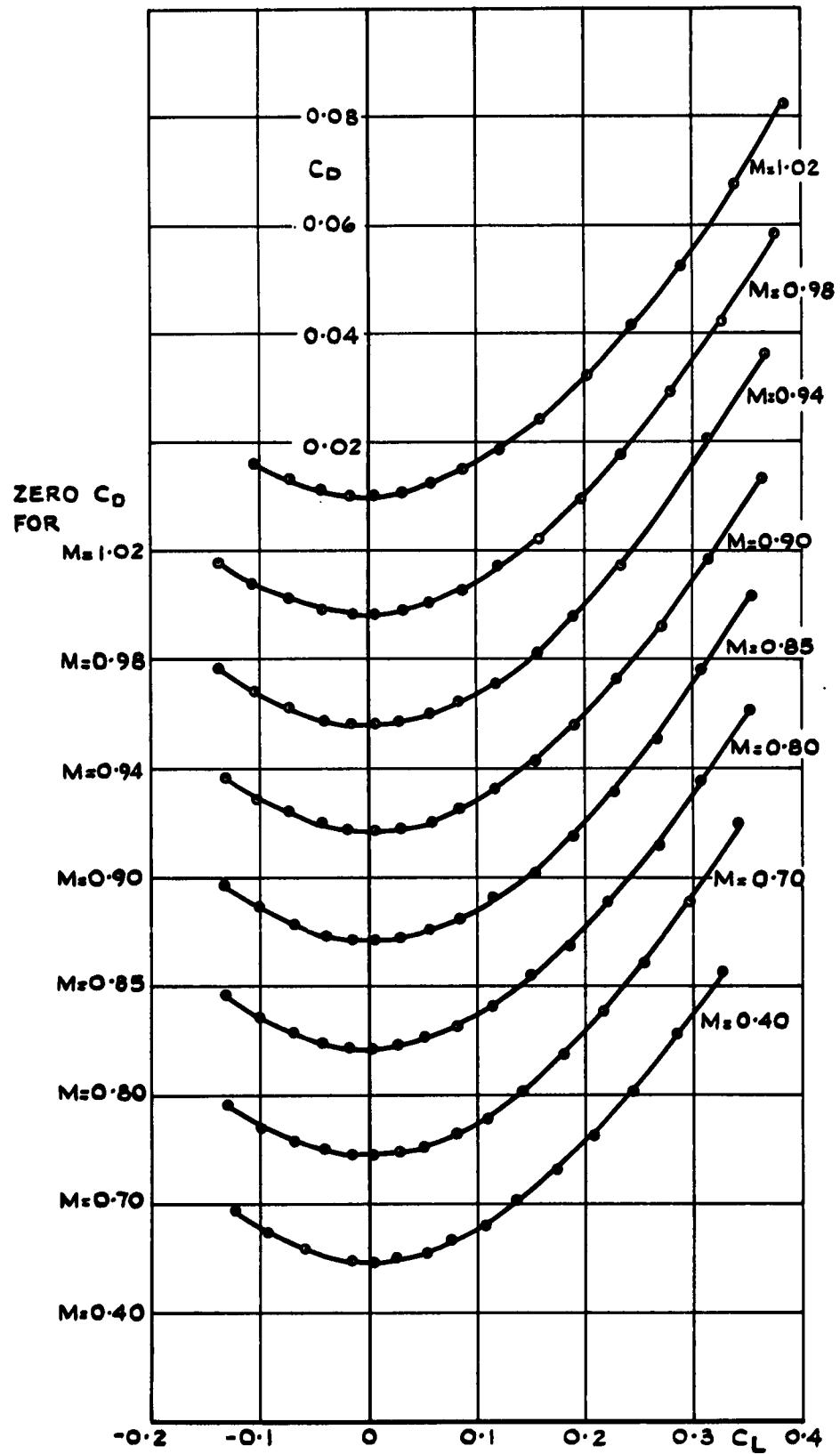
FIG.11b. OIL FLOW PHOTOGRAPHS. WING I.

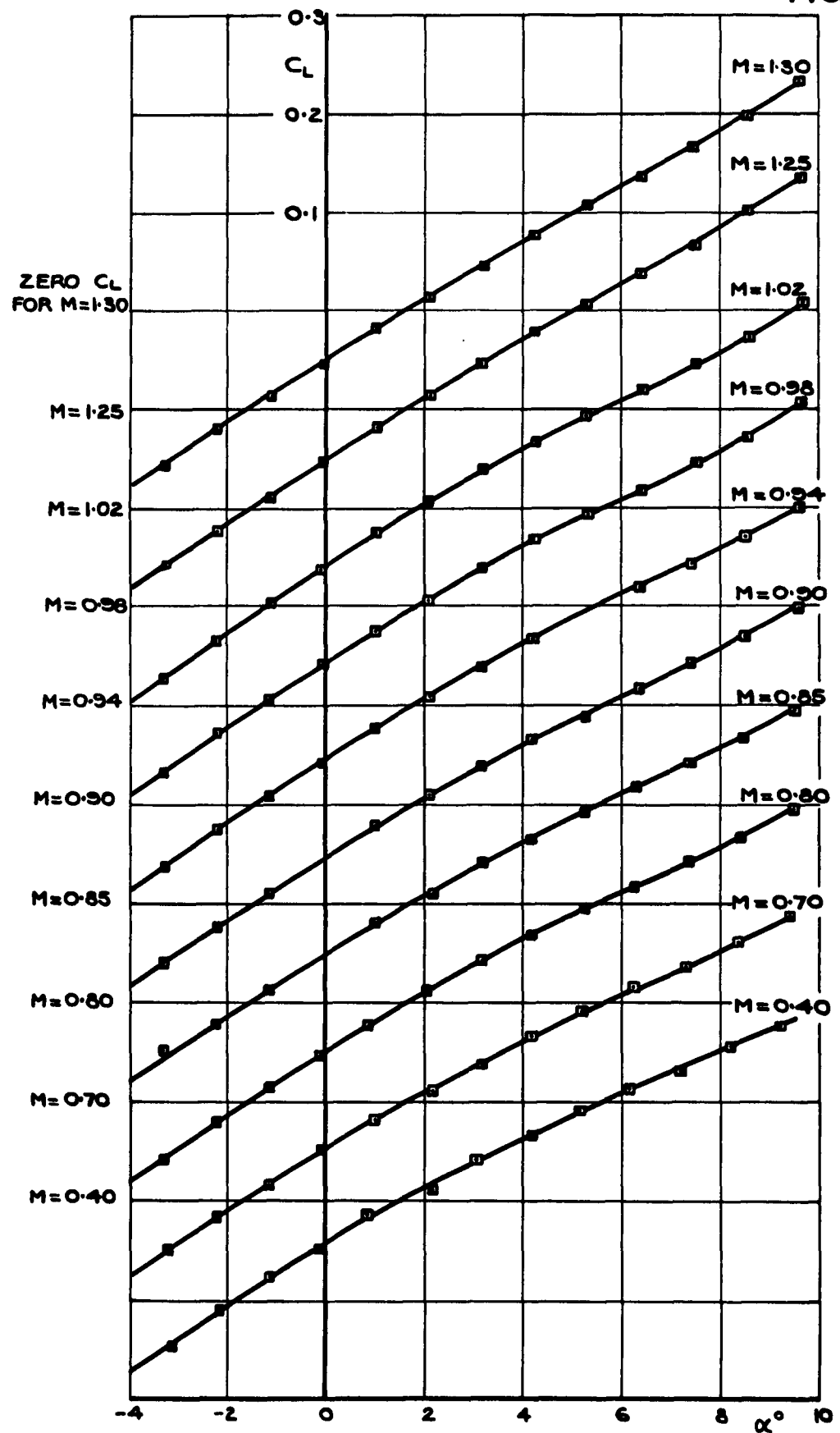
$\alpha \approx 4^\circ$

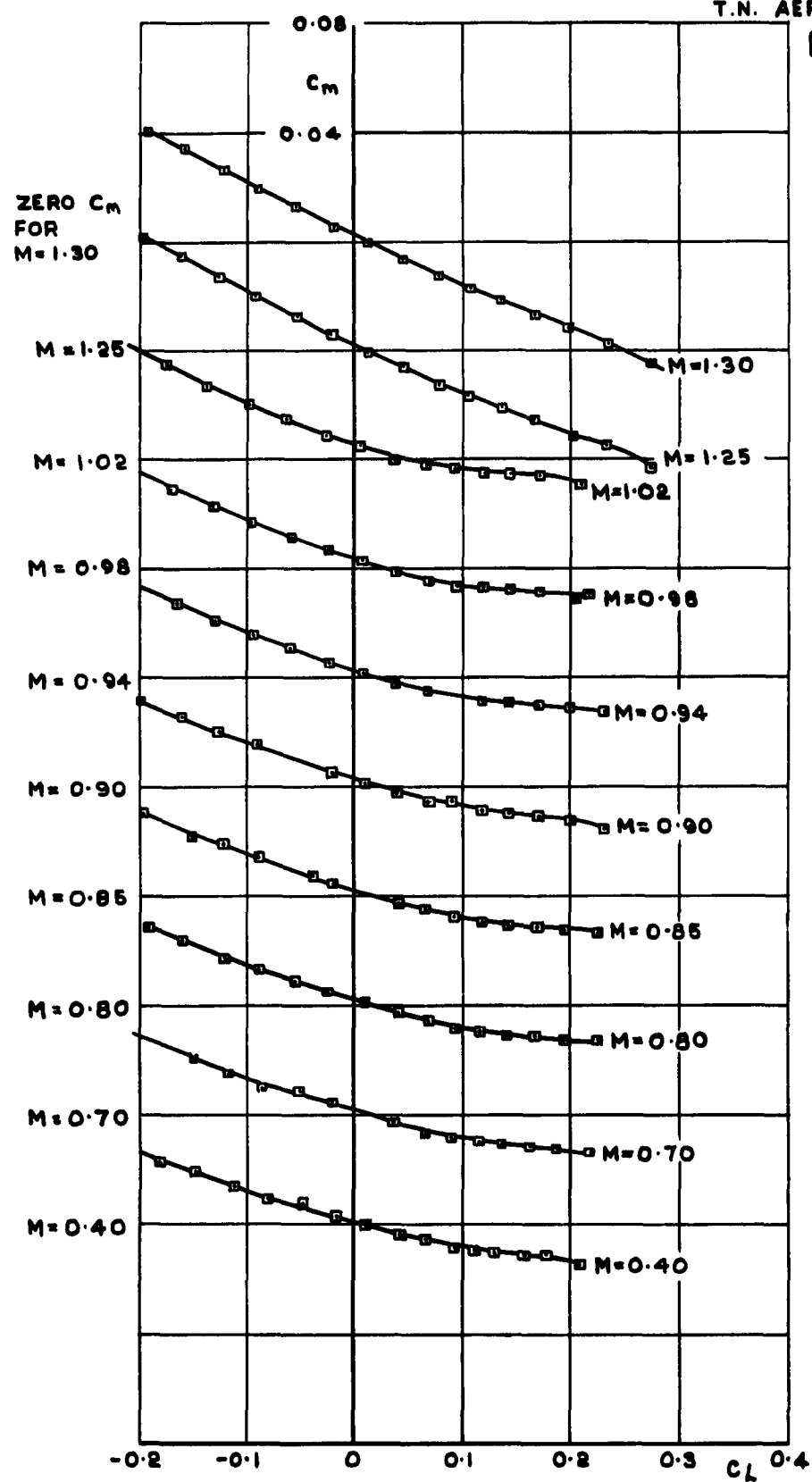
FIG. 12. VARIATION OF  $C_L$  WITH  $\alpha$  : WING I.

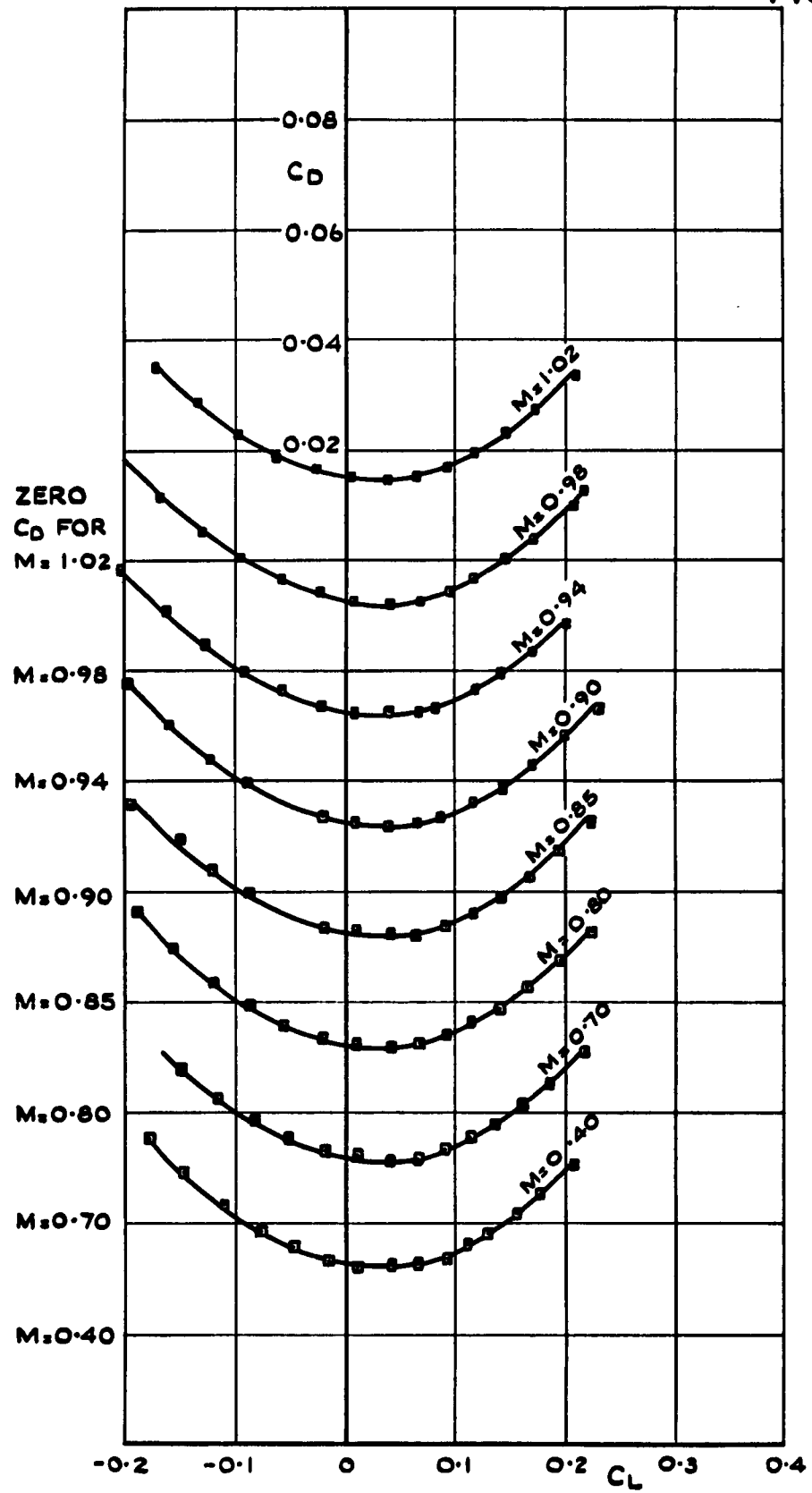


FIG. 13. VARIATION OF  $C_m$  WITH  $C_L$  : WING I.

FIG. 14. VARIATION OF  $C_D$  WITH  $C_L$  : WING I.

FIG.15. VARIATION OF  $C_L$  WITH  $\alpha$ : WING 2

FIG. 16. VARIATION OF  $C_m$  WITH  $C_L$  : WING 2.

FIG. 17. VARIATION OF  $C_D$  WITH  $C_L$  : WING 2.

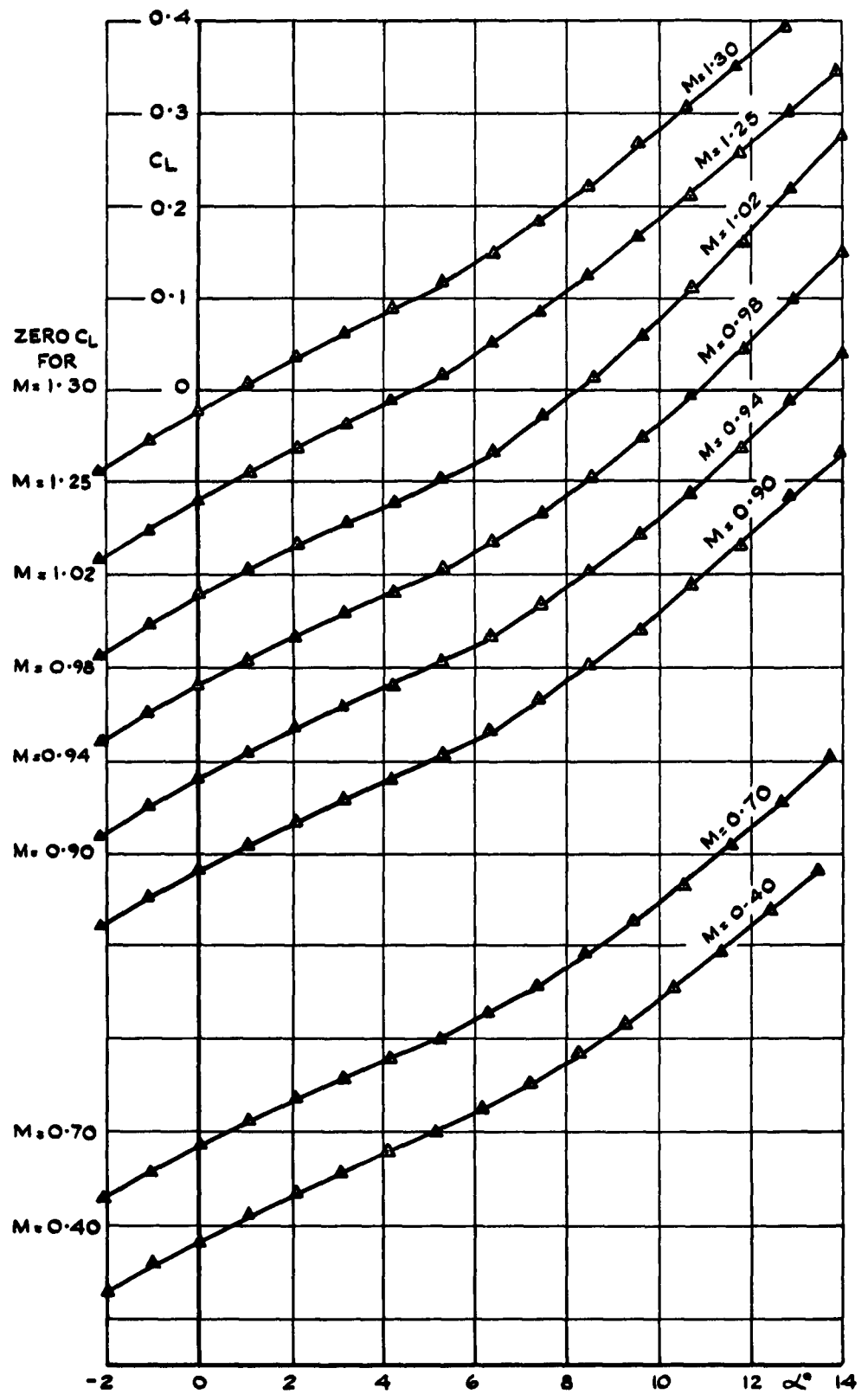
FIG.18. VARIATION OF  $C_L$  WITH  $\alpha$  : WING 3.

FIG. 19

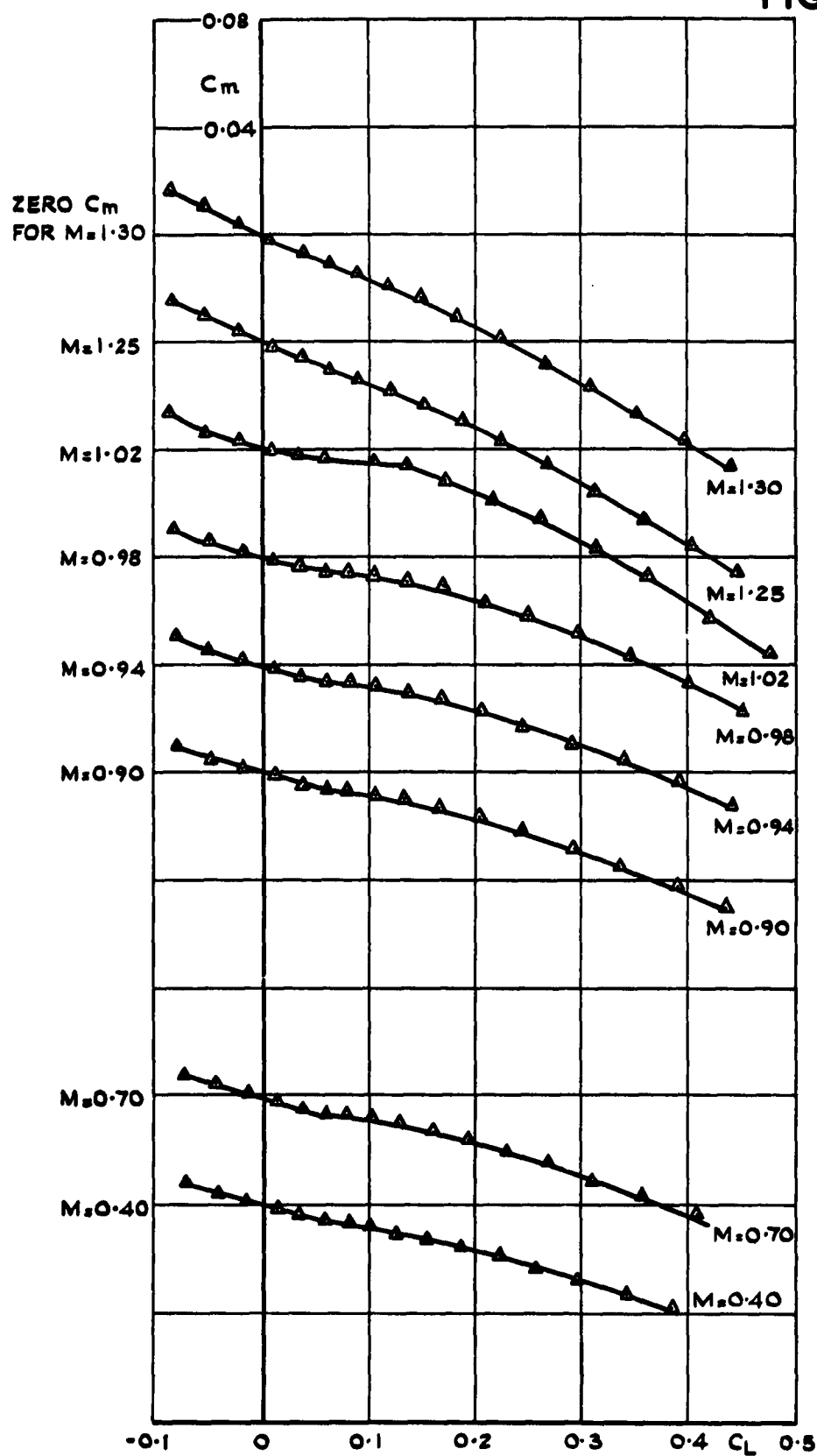
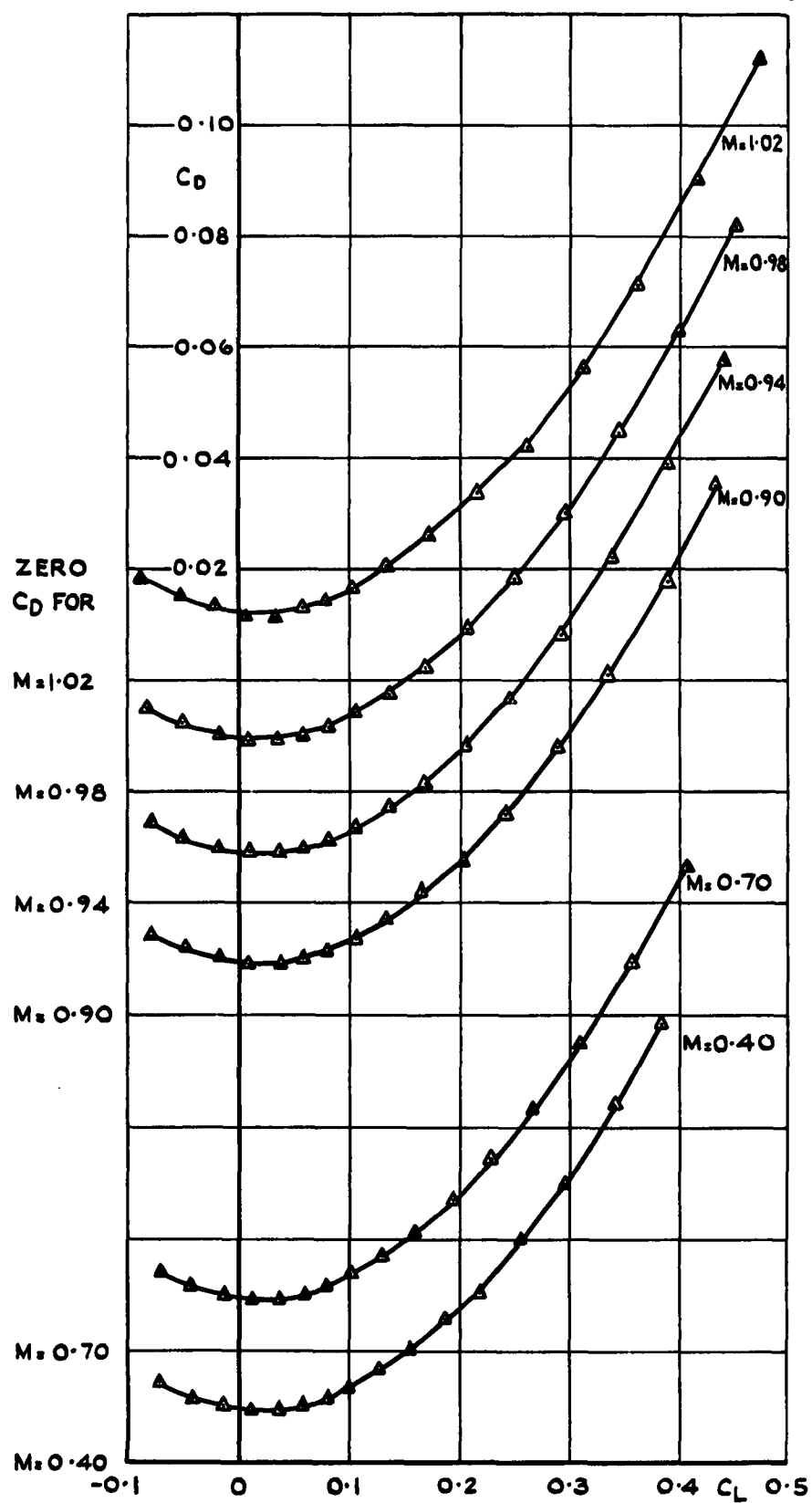


FIG.19. VARIATION OF  $C_m$  WITH  $C_L$  :  
WING 3.

FIG. 20 VARIATION OF  $C_D$  WITH  $C_L$  : WING 3.



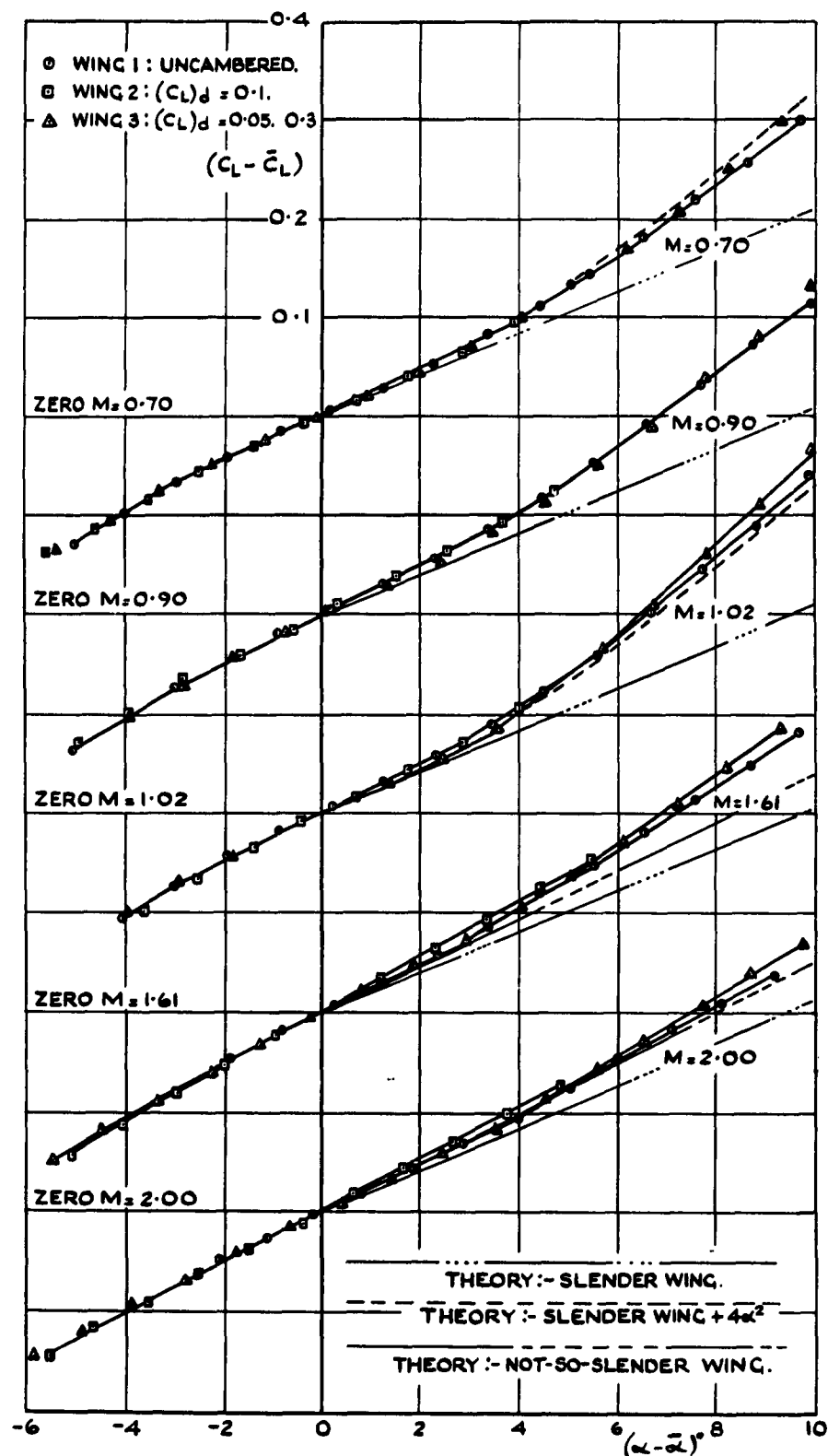


FIG. 21. VARIATION OF  $(C_L - \bar{C}_L)$  WITH  $(\alpha - \bar{\alpha})$   
WINGS 1, 2 AND 3.

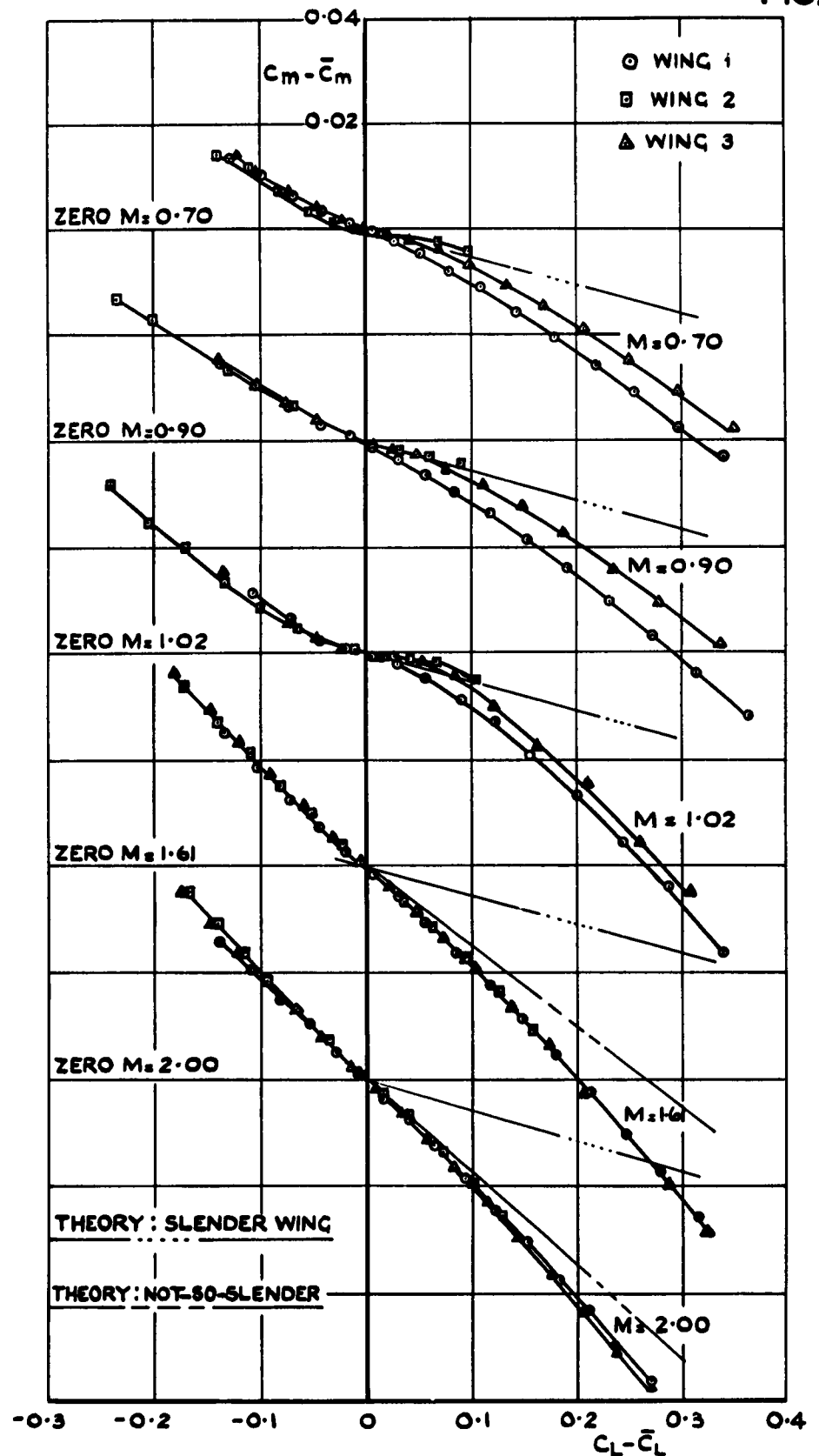


FIG. 22. VARIATION OF  $(C_m - \bar{C}_m)$  WITH  $(C_L - \bar{C}_L)$   
WINGS 1, 2 AND 3.

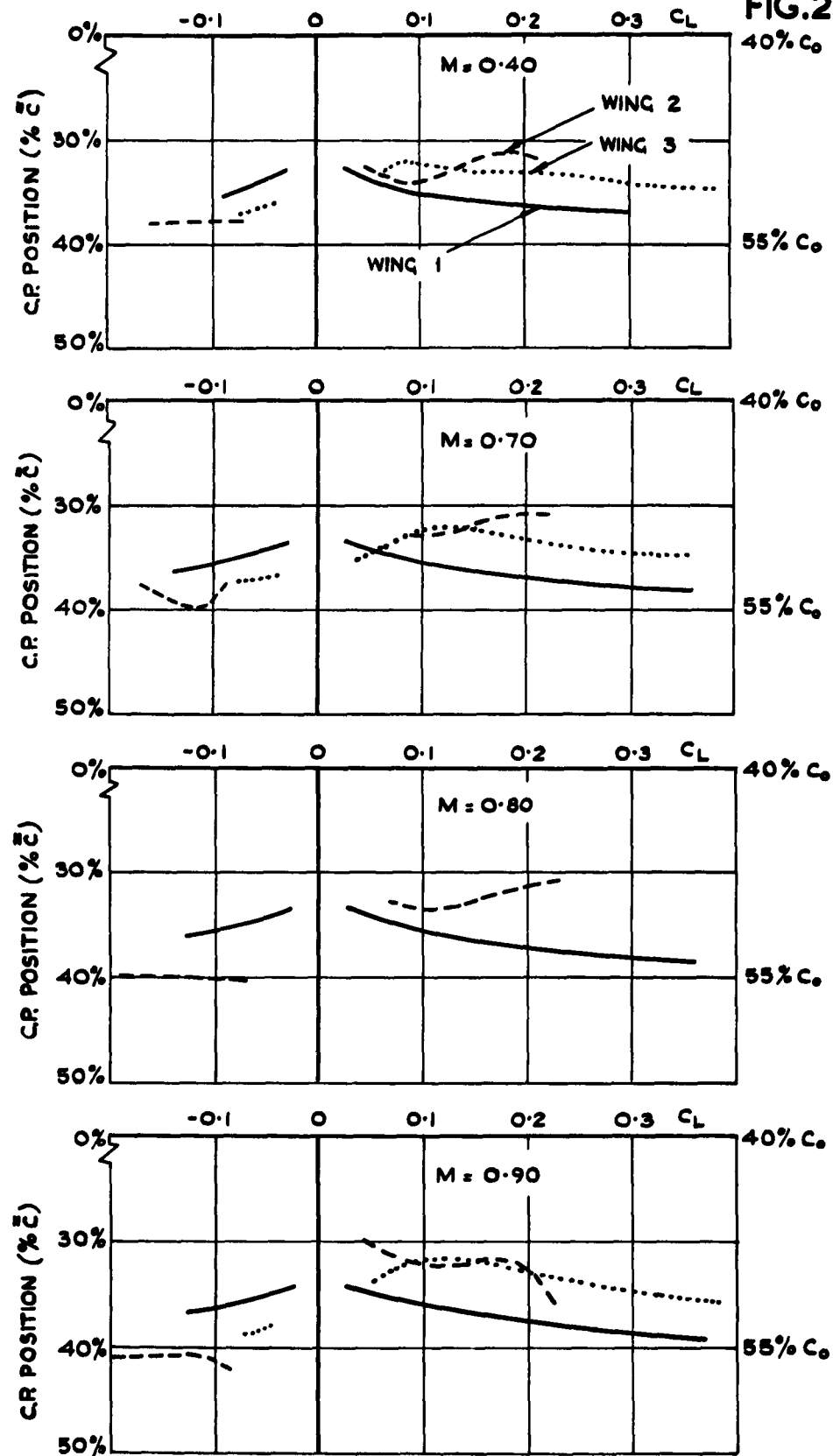


FIG. 23 (a) VARIATION OF CENTRE OF PRESSURE POSITION WITH  $C_L$  AT CONSTANT MACH NUMBER : WINGS 1, 2 AND 3.

FIG.23(b)

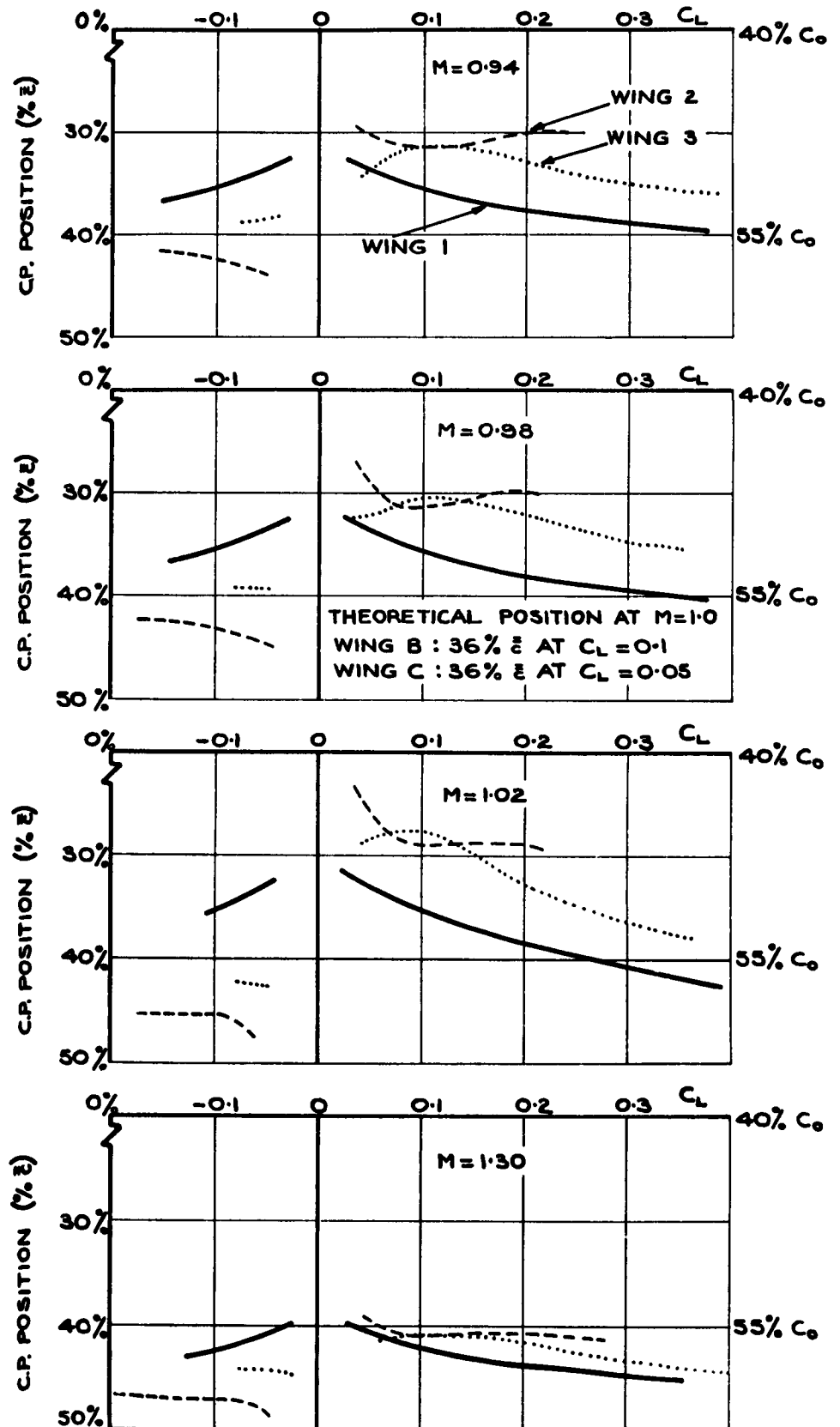


FIG.23(b) VARIATION OF CENTRE OF PRESSURE POSITION WITH  $C_L$  AT CONSTANT MACH NUMBER, WINGS 1,2 AND 3.

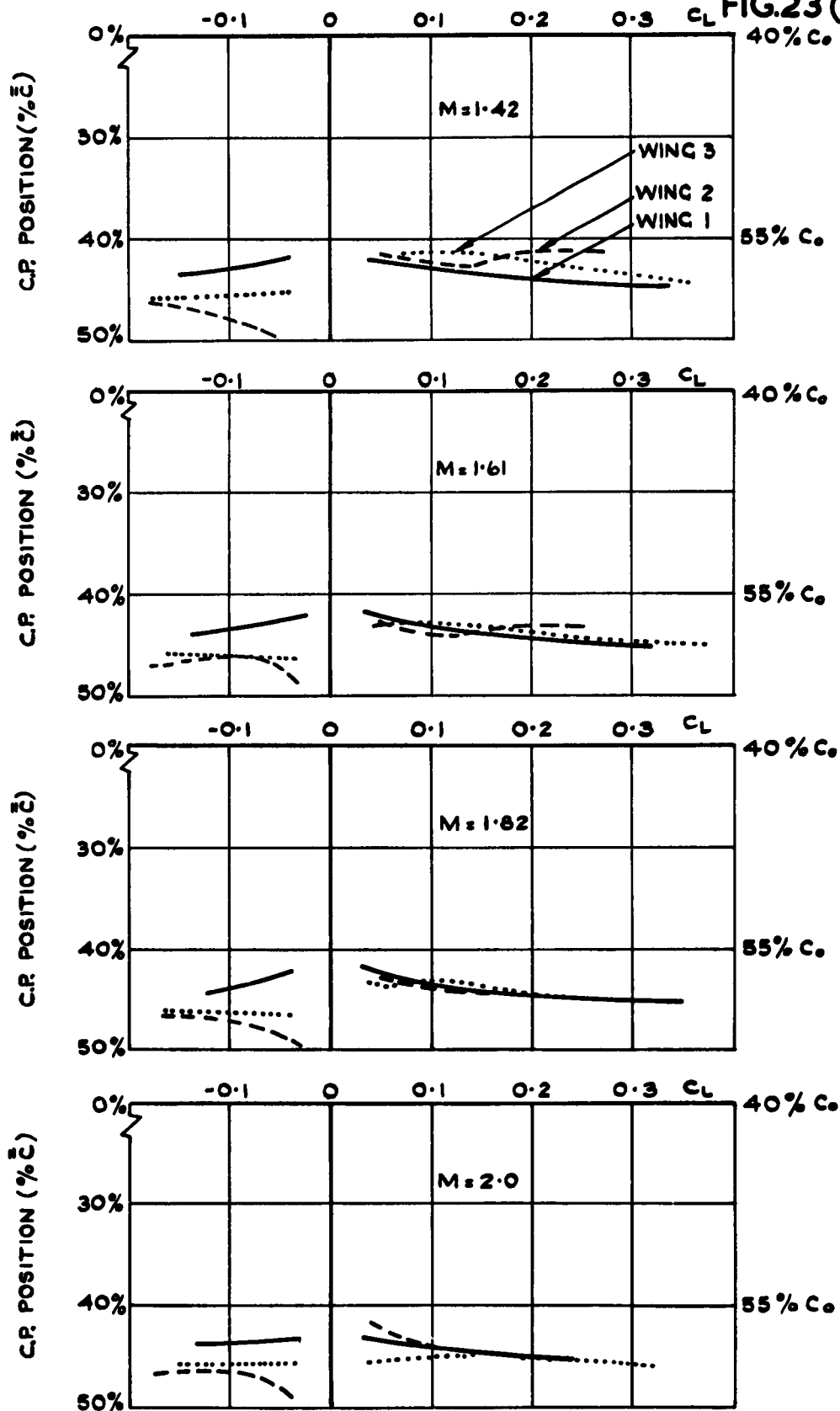


FIG. 23 (c) VARIATION OF CENTRE OF PRESSURE POSITION WITH  $C_L$  AT CONSTANT MACH NUMBER : WINGS 1, 2 AND 3.

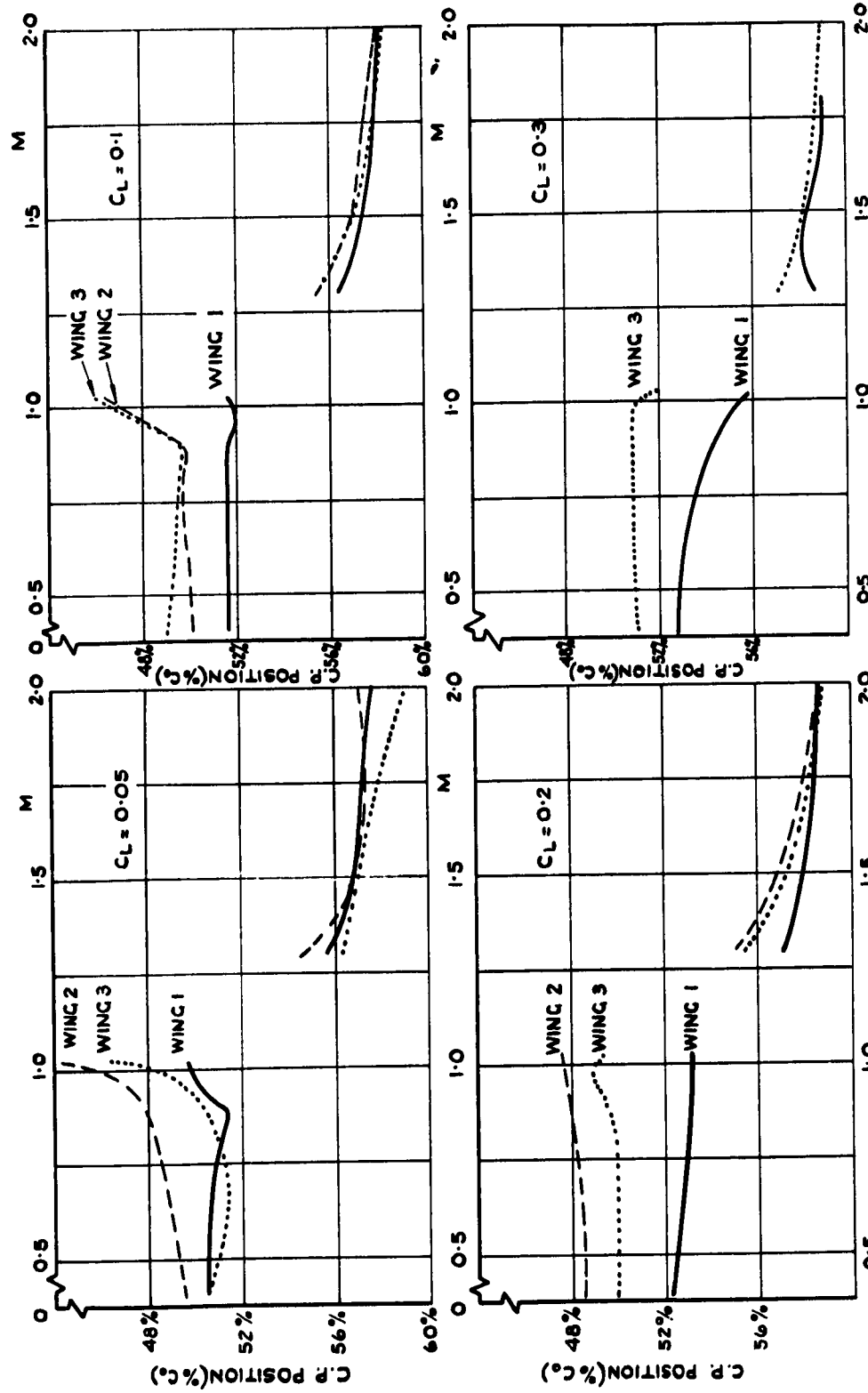


FIG. 24. VARIATION OF CENTRE OF PRESSURE WITH MACH NUMBER, POSITION AT FIXED  $C_L$ :  
WINGS 1, 2 AND 3.

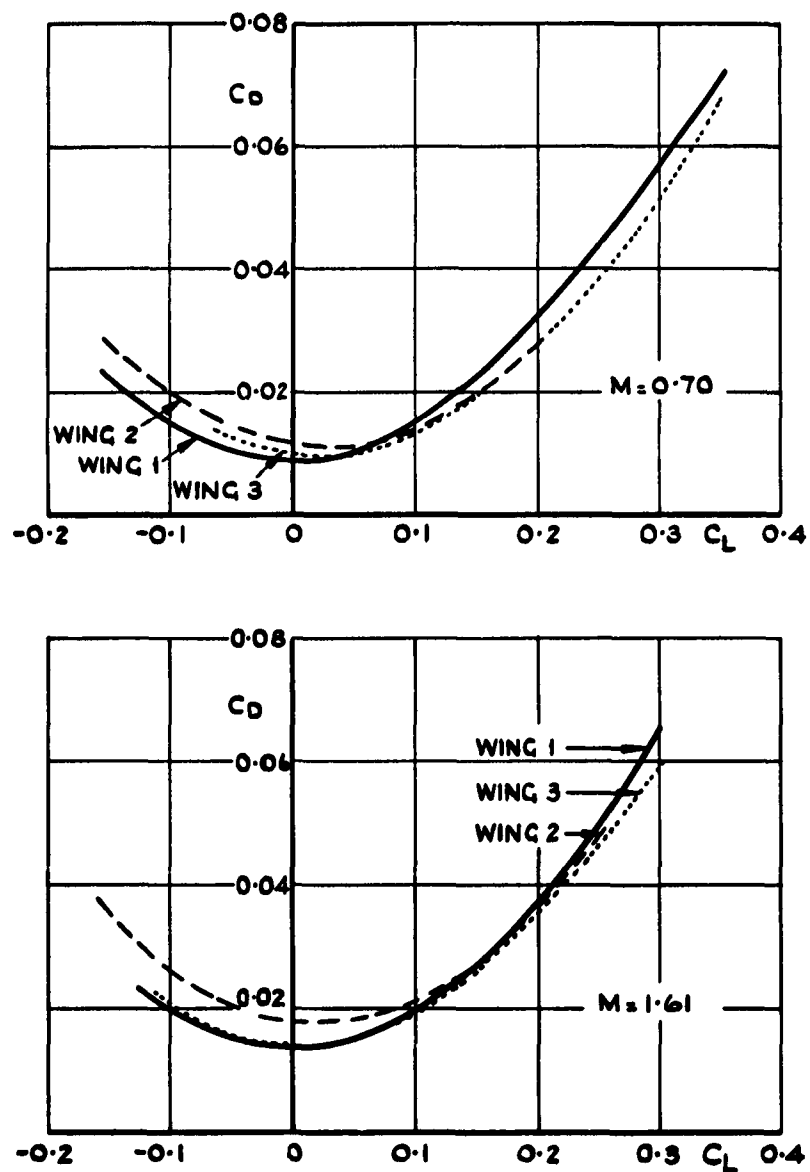


FIG. 25. COMPARISON OF DRAG POLARS OF WINGS 1,2 AND 3.

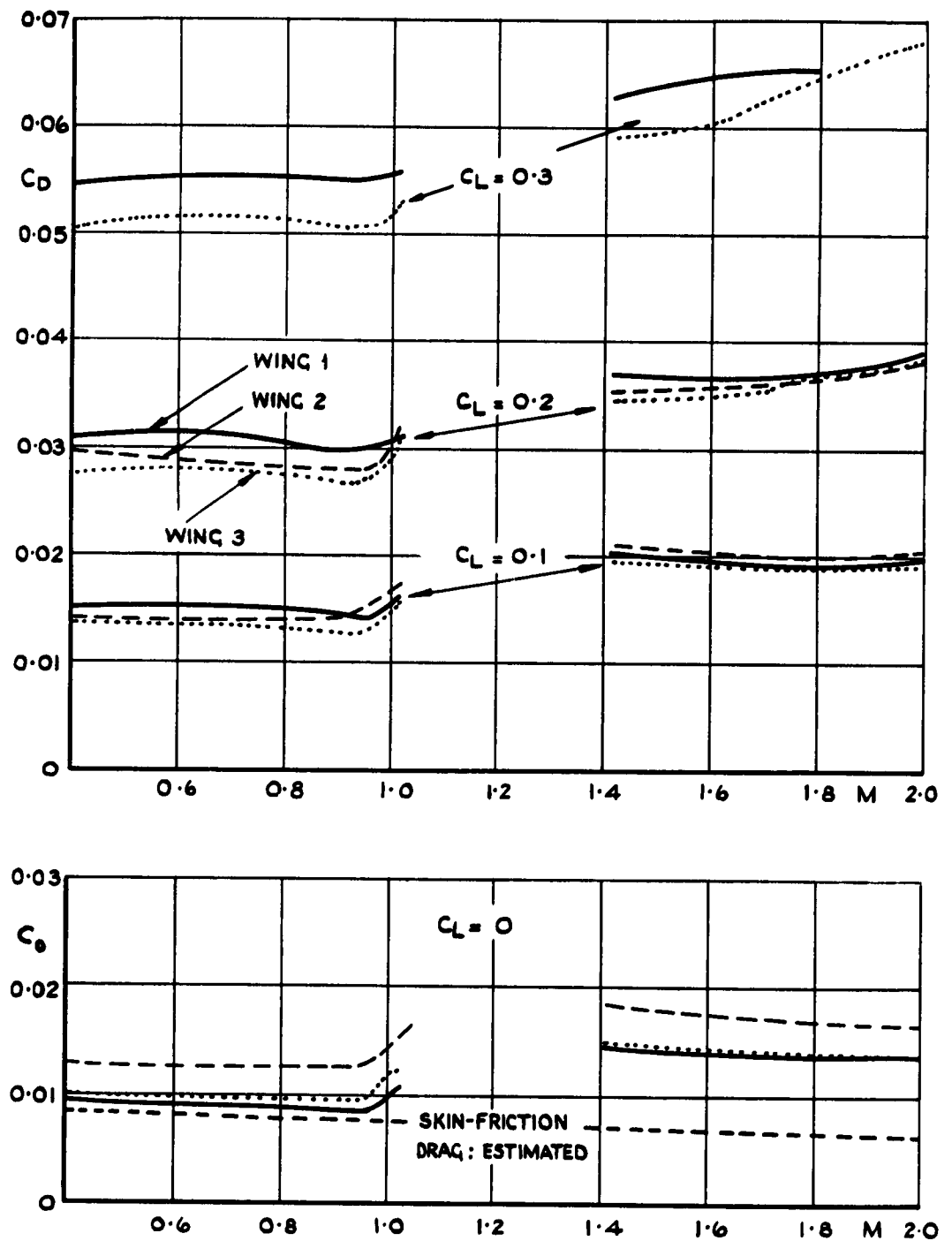


FIG. 26. VARIATION WITH MACH NUMBER OF THE DRAG AT FIXED  $C_L$  : WINGS 1, 2 AND 3.



FIG. 27(a)

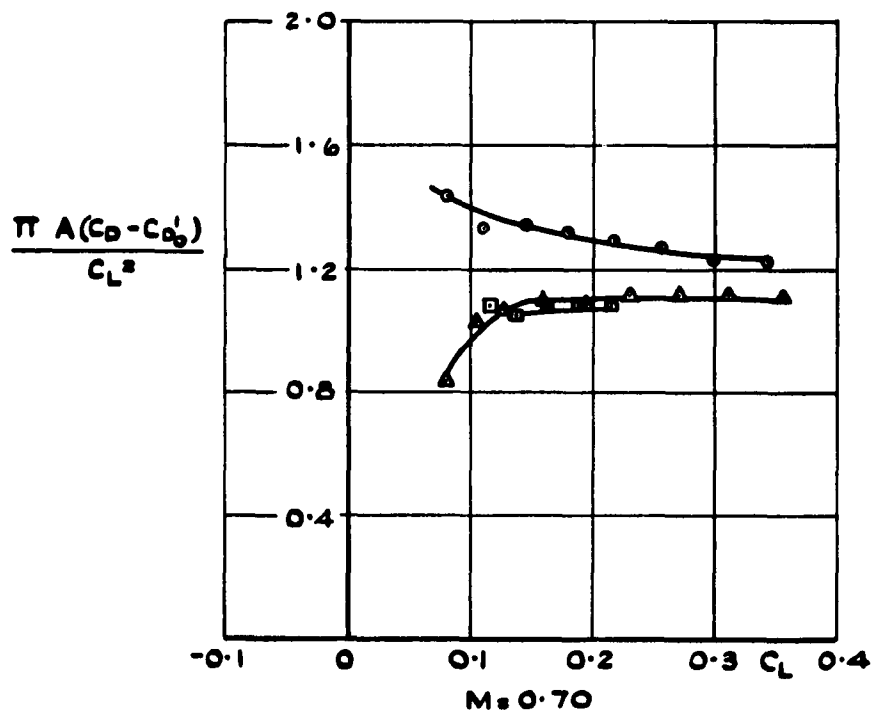
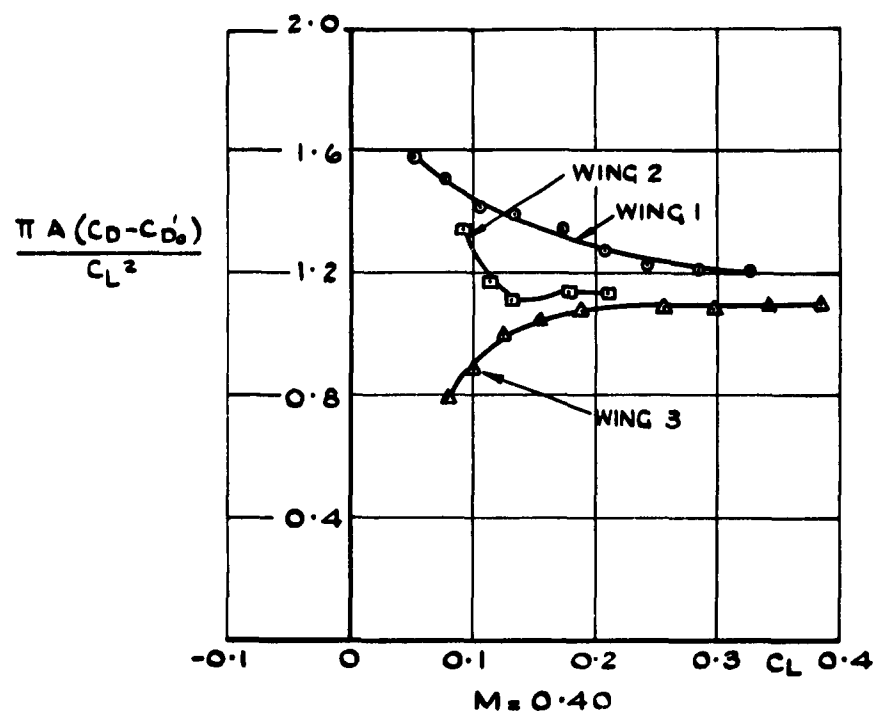


FIG. 27(a) VARIATION WITH  $C_L$  OF THE  
LIFT-DEPENDENT DRAG FACTOR :  
WINGS 1,2 AND 3.

FIG. 27(b)

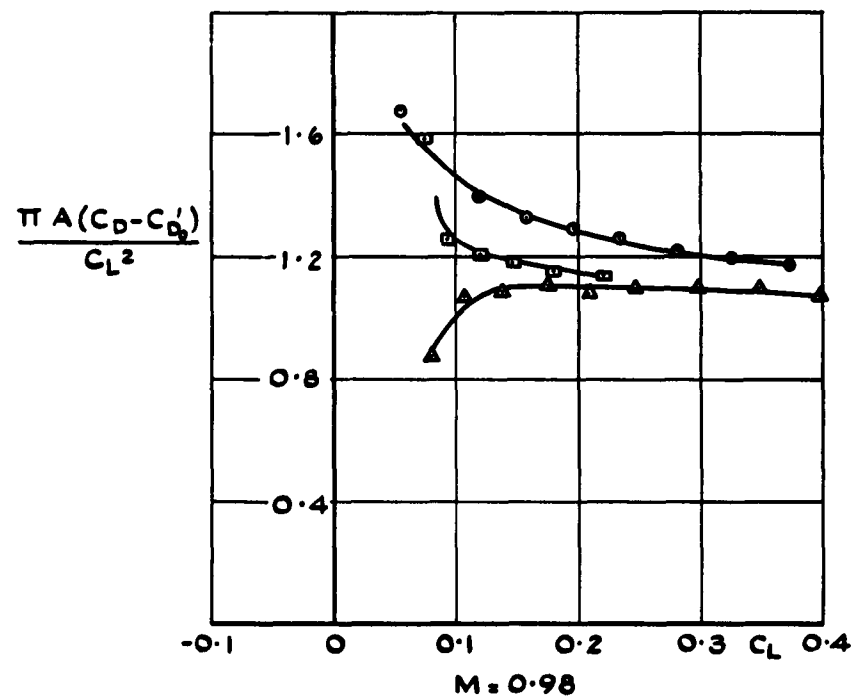
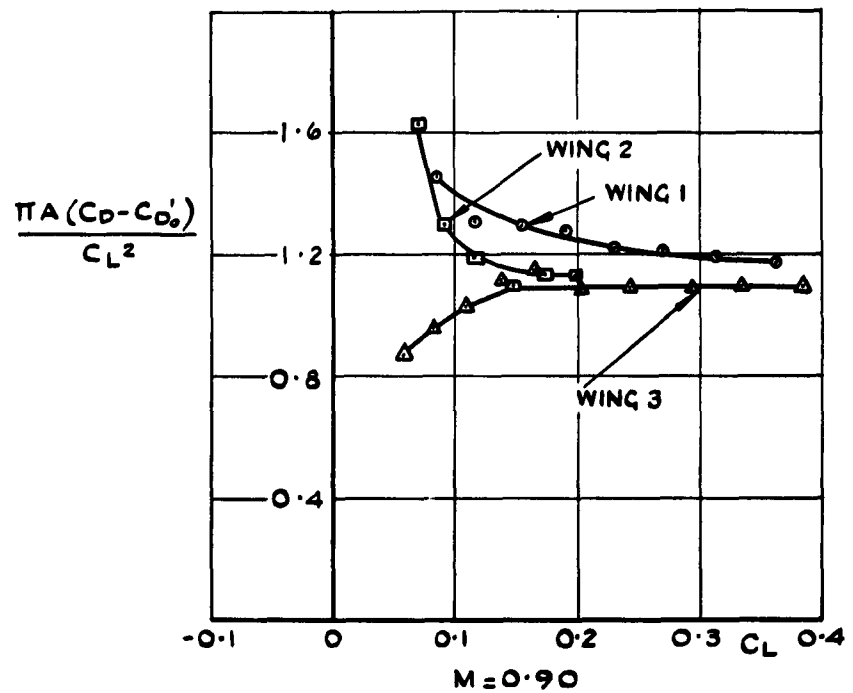


FIG. 27(b) VARIATION WITH  $C_L$  OF THE  
LIFT-DEPENDENT DRAG FACTOR :  
WINGS 1, 2 AND 3.

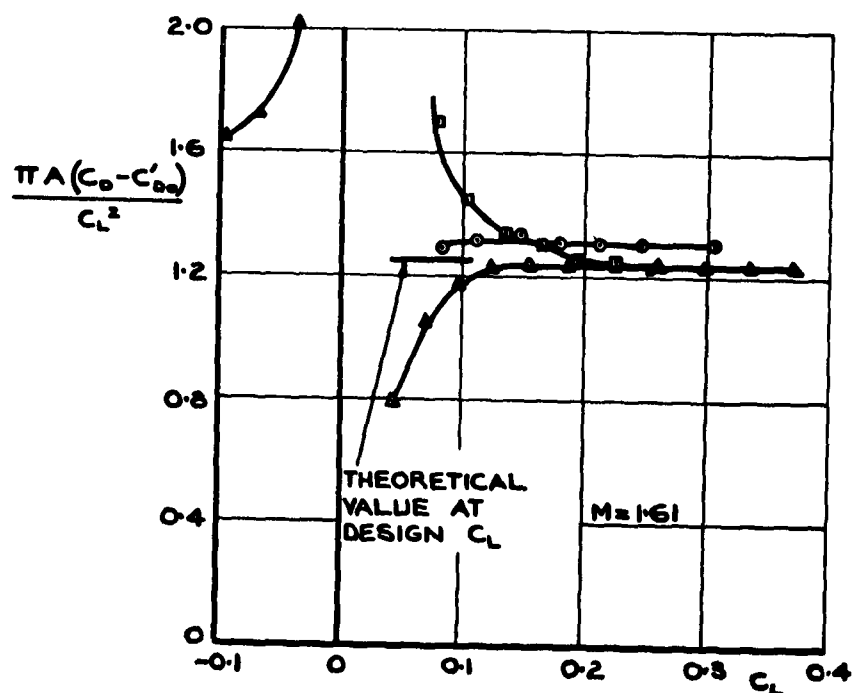
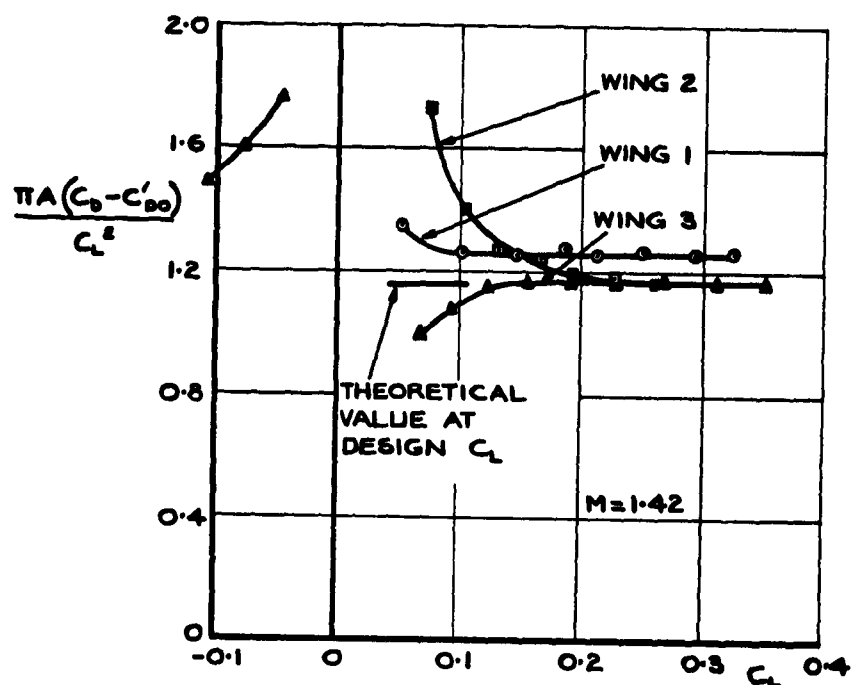


FIG. 27(c) VARIATION WITH  $C_L$  OF THE LIFT-DEPENDENT DRAG FACTOR : WINGS 1, 2 AND 3.

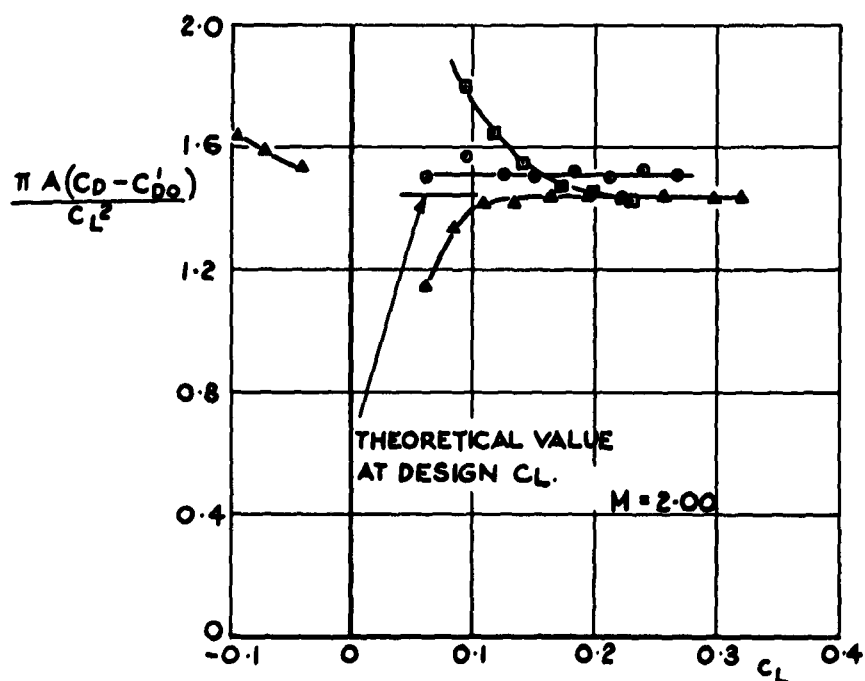
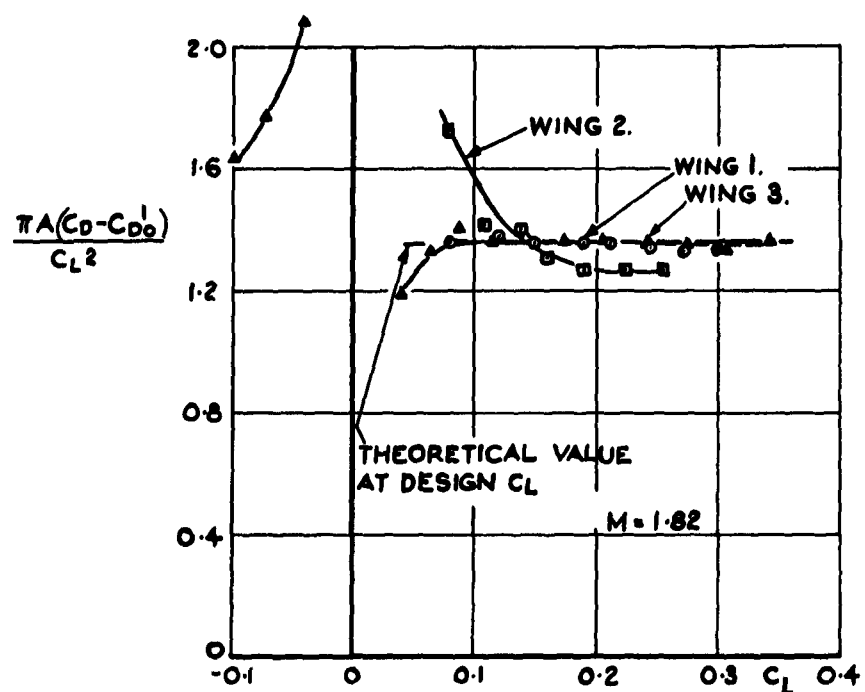


FIG.27(d) VARIATION WITH  $C_L$  OF THE  
LIFT DEPENDENT DRAG FACTOR:  
WINGS 1, 2 & 3.

FIG. 28

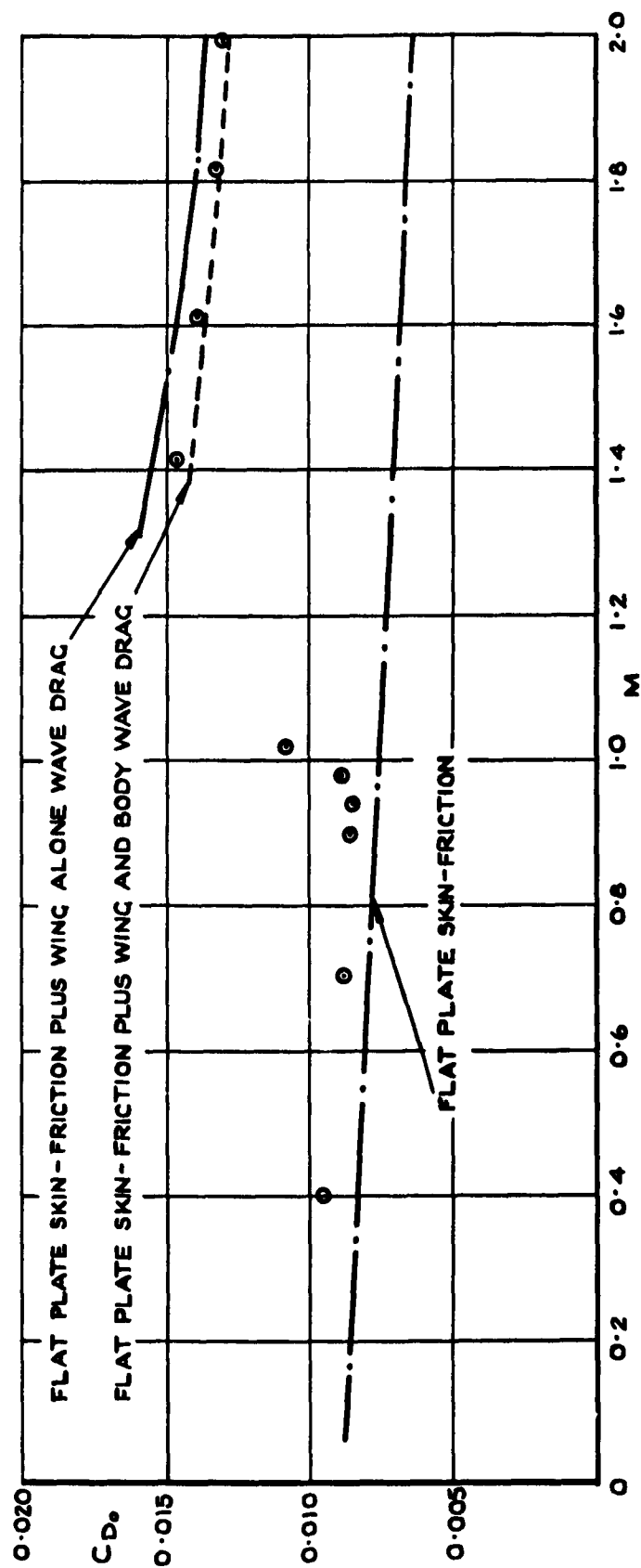
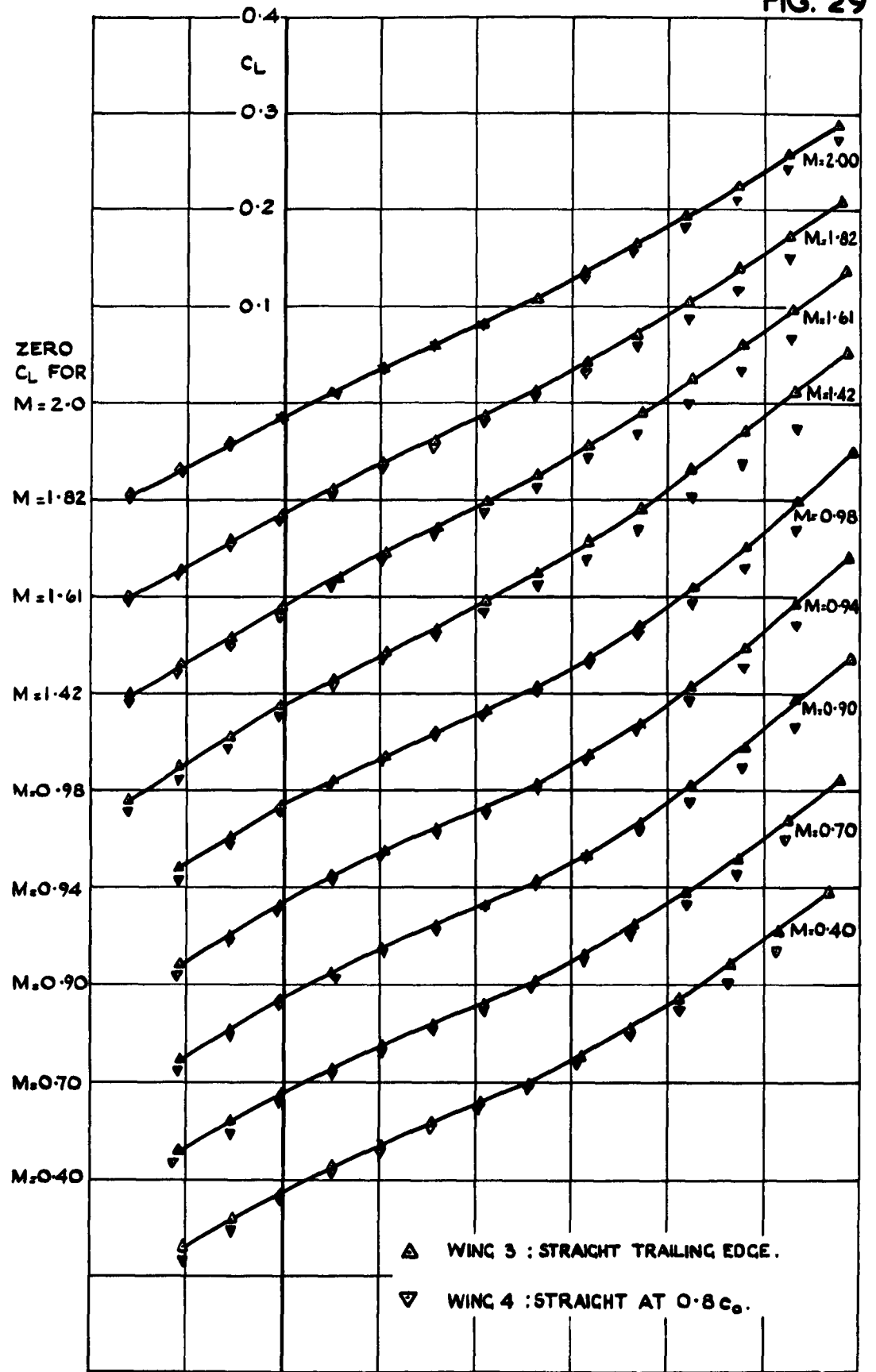
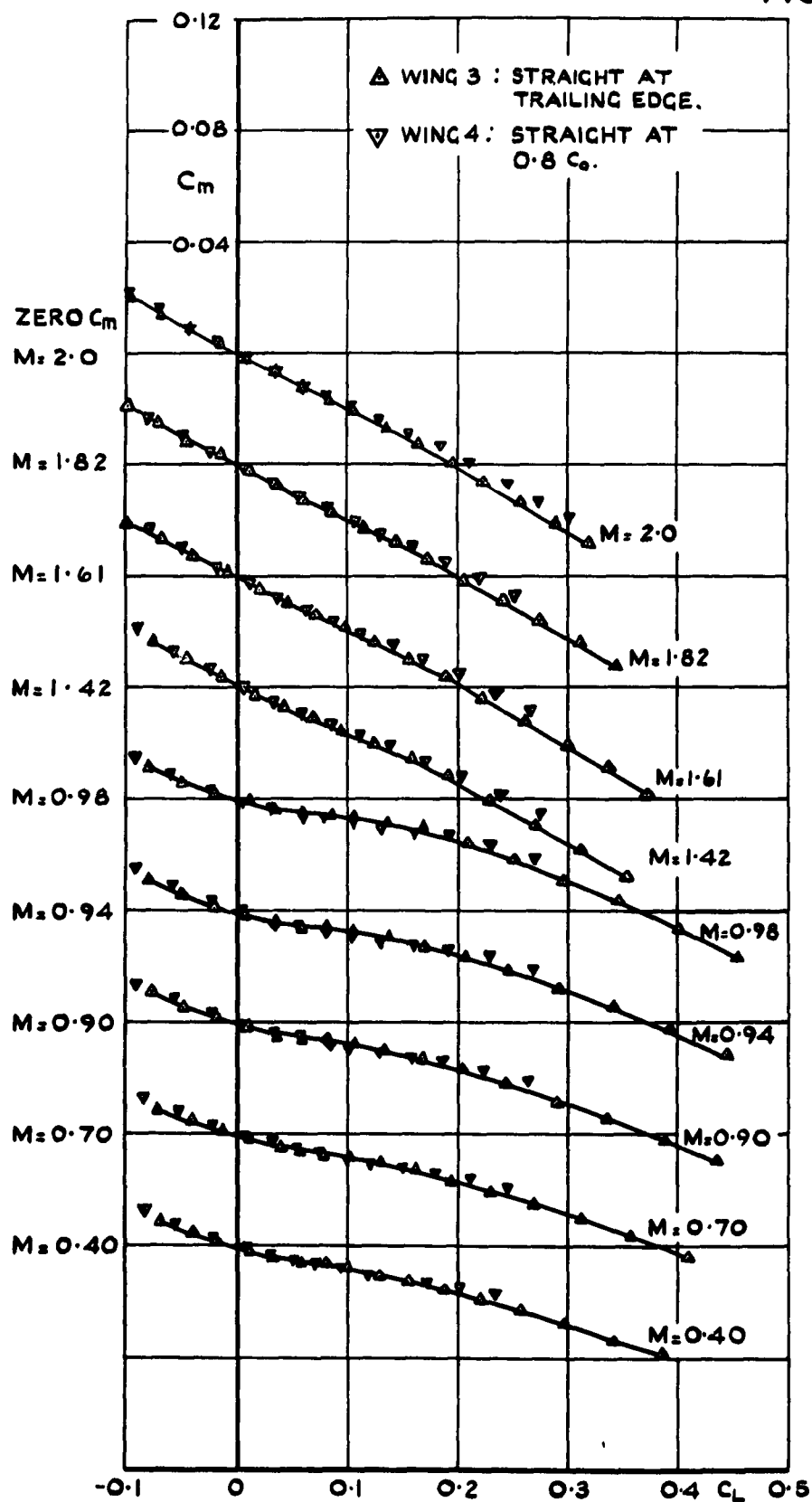
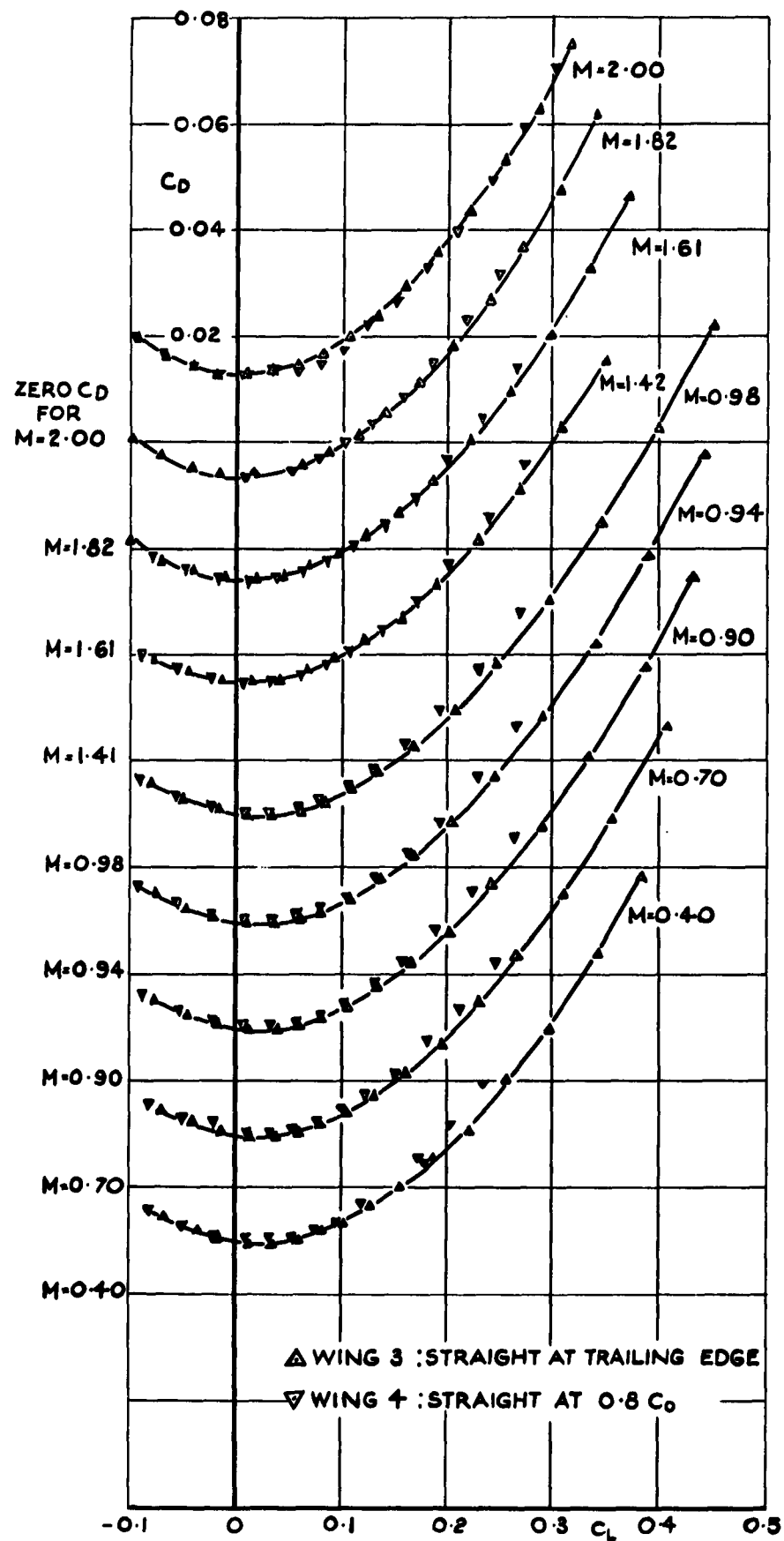


FIG. 28. COMPARISON OF ZERO LIFT DRAG OF WING WITH THEORY.

FIG.29. VARIATION OF  $C_L$  WITH  $\alpha$  : WINGS 3 AND 4.

FIG.30. VARIATION OF  $C_m$  WITH  $C_L$  : WINGS 3 AND 4.

FIG.31. VARIATION OF  $C_D$  WITH  $C_L$ : WINGS 3 & 4.



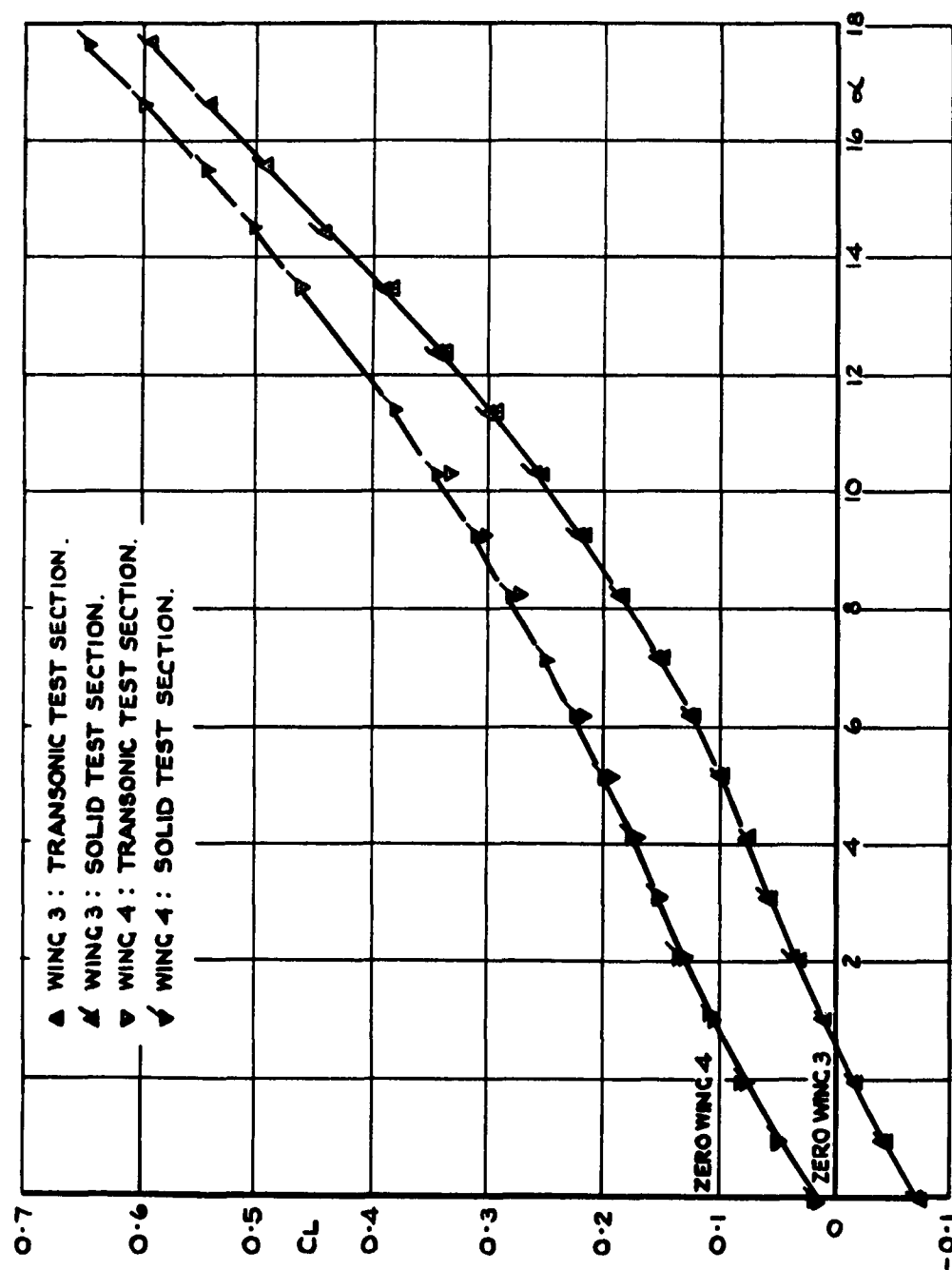


FIG. 32 VARIATION OF  $C_L$  WITH  $\alpha$ :  $M=0.4$  : WINGS 3 AND 4.

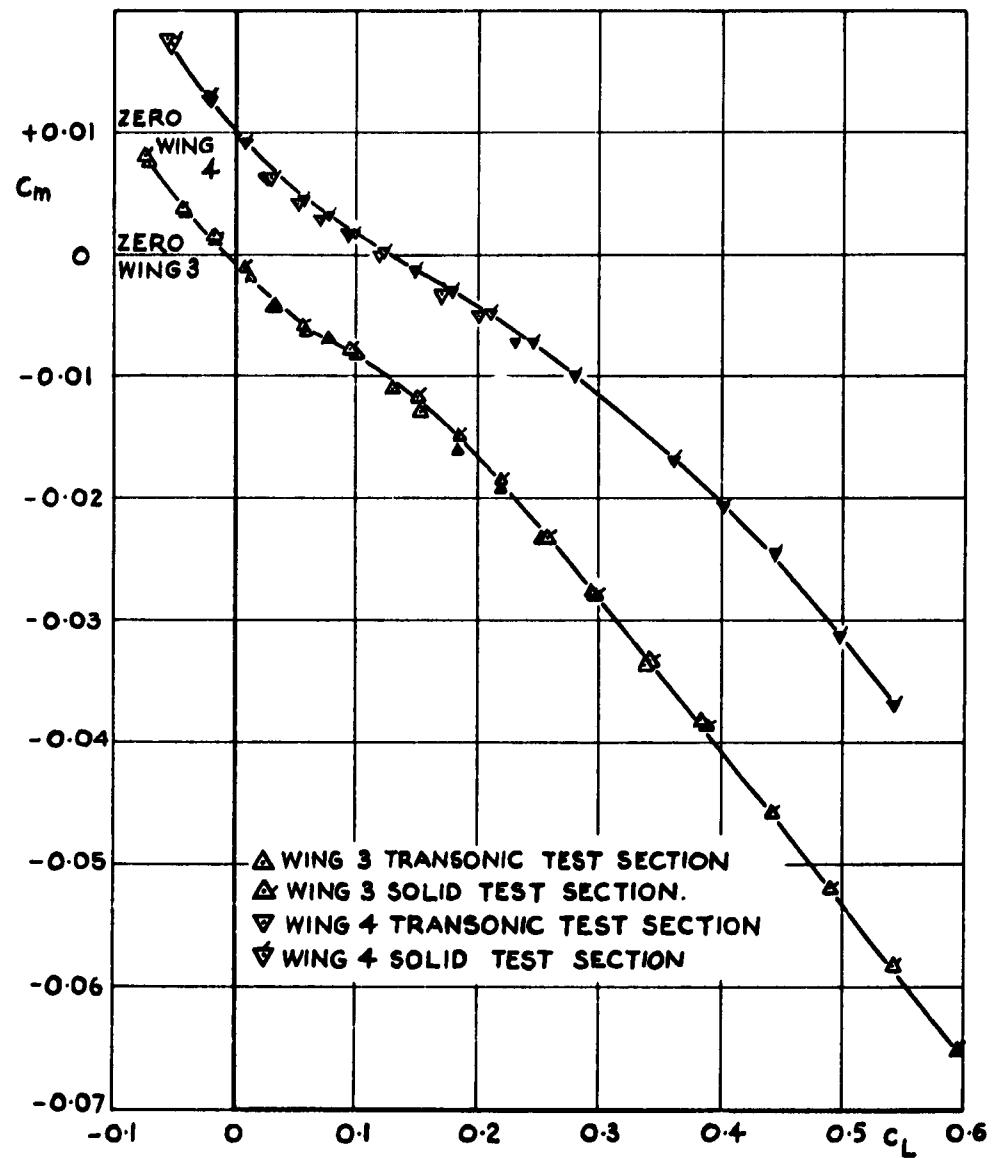


FIG.33. VARIATION OF  $C_m$  WITH  $C_L$ :  $M=0.4$ ,  
WINGS 3 & 4.

FIG 34.

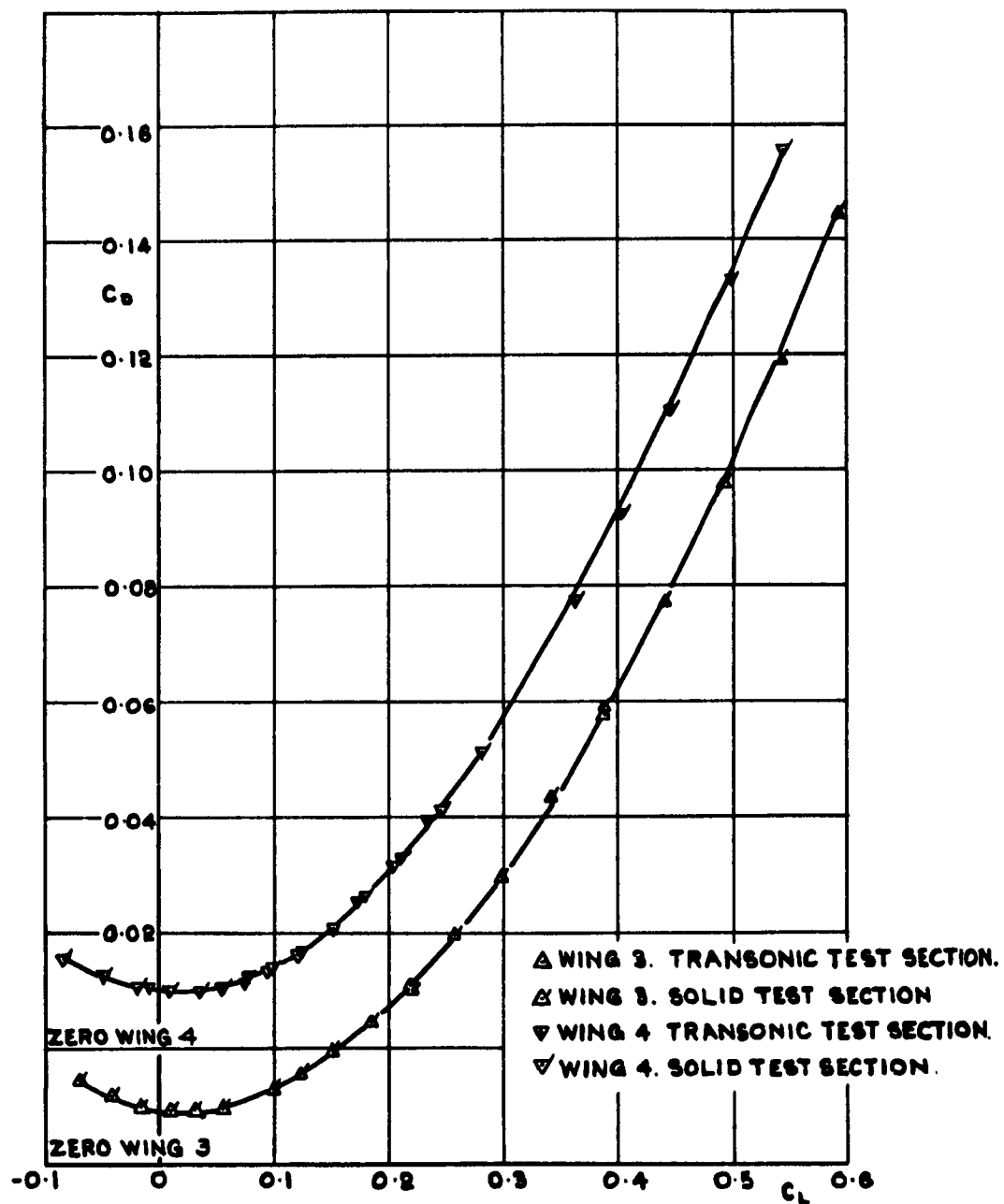


FIG. 34. VARIATION OF  $C_D$  WITH  $C_L$  :  $M = 0.4$  :  
WINGS 3 AND 4.

# DETACHABLE ABSTRACT CARDS

These abstract cards are inserted in Reports and Technical Notes for the convenience of Librarians and others who need to maintain an Information Index.

<p>UNCLASSIFIED</p> <p>Technical Note No. Aero 2803 Royal Aircraft Establishment, Bedford</p> <p>533.693.3: 533.6.032: 533.6.013.1: 533.6.011.34/5</p>	<p>UNCLASSIFIED</p> <p>Technical Note No. Aero 2803 Royal Aircraft Establishment, Bedford</p> <p>533.693.3: 533.6.032: 533.6.013.1: 533.6.011.34/5</p>
<p>FURTHER EXPERIMENTAL INVESTIGATIONS OF THE CHARACTERISTICS OF CAMBERED GOOTHIC WINGS AT MACH NUMBERS FROM 0.4 TO 2.0. Squire, L.C. December, 1961.</p> <p>The wind tunnel tests on cambered gothic wings reported in Reports and Memoranda No.3211 have been extended to include the effects of changes in design lift coefficient and of changes in spanwise camber without changes in camber incidence distribution.</p> <p>It was found that the camber was successful in that the flow was attached over the whole wing at the design lift. Also at the design lift the lift-dependent drag was close to the predicted values. However, the lift-dependent drag of the uncambered wing was also close to this value so that the benefit of camber on lift/drag ratio was very small. At</p>	<p>FURTHER EXPERIMENTAL INVESTIGATIONS OF THE CHARACTERISTICS OF CAMBERED GOOTHIC WINGS AT MACH NUMBERS FROM 0.4 TO 2.0. Squire, L.C. December, 1961.</p> <p>The wind tunnel tests on cambered gothic wings reported in Reports and Memoranda No.3211 have been extended to include the effects of changes in design lift coefficient and of changes in spanwise camber without changes in camber incidence distribution.</p> <p>It was found that the camber was successful in that the flow was attached over the whole wing at the design lift. Also at the design lift the lift-dependent drag was close to the predicted values. However, the lift-dependent drag of the uncambered wing was also close to this value so that the benefit of camber on lift/drag ratio was very small. At</p>
<p>UNCLASSIFIED</p> <p>Technical Note No. Aero 2803 Royal Aircraft Establishment, Bedford</p> <p>533.693.3: 533.6.032: 533.6.013.1: 533.6.011.34/5</p>	<p>UNCLASSIFIED</p> <p>Technical Note No. Aero 2803 Royal Aircraft Establishment, Bedford</p> <p>533.693.3: 533.6.032: 533.6.013.1: 533.6.011.34/5</p>
<p>FURTHER EXPERIMENTAL INVESTIGATIONS OF THE CHARACTERISTICS OF CAMBERED GOOTHIC WINGS AT MACH NUMBERS FROM 0.4 TO 2.0. Squire, L.C. December, 1961.</p> <p>The wind tunnel tests on cambered gothic wings reported in Reports and Memoranda No.3211 have been extended to include the effects of changes in design lift coefficient and of changes in spanwise camber without changes in camber incidence distribution.</p> <p>It was found that the camber was successful in that the flow was attached over the whole wing at the design lift. Also at the design lift the lift-dependent drag was close to the predicted values. However, the lift-dependent drag of the uncambered wing was also close to this value so that the benefit of camber on lift/drag ratio was very small. At</p>	<p>FURTHER EXPERIMENTAL INVESTIGATIONS OF THE CHARACTERISTICS OF CAMBERED GOOTHIC WINGS AT MACH NUMBERS FROM 0.4 TO 2.0. Squire, L.C. December, 1961.</p> <p>The wind tunnel tests on cambered gothic wings reported in Reports and Memoranda No.3211 have been extended to include the effects of changes in design lift coefficient and of changes in spanwise camber without changes in camber incidence distribution.</p> <p>It was found that the camber was successful in that the flow was attached over the whole wing at the design lift. Also at the design lift the lift-dependent drag was close to the predicted values. However, the lift-dependent drag of the uncambered wing was also close to this value so that the benefit of camber on lift/drag ratio was very small. At</p>

UNCLASSIFIED

subsonic speeds the cambered wings were less stable than the uncambered wing; also the changes of stability with incidence and Mach number were greater, particularly near  $M = 1.0$ .

Changes in spanwise camber without changes in incidence distribution, do not alter the force characteristics near the design lift, but do alter the off-design characteristics.

UNCLASSIFIED

subsonic speeds the cambered wings were less stable than the uncambered wing; also the changes of stability with incidence and Mach number were greater, particularly near  $M = 1.0$ .

Changes in spanwise camber without changes in incidence distribution, do not alter the force characteristics near the design lift, but do alter the off-design characteristics.

UNCLASSIFIED

subsonic speeds the cambered wings were less stable than the uncambered wing; also the changes of stability with incidence and Mach number were greater, particularly near  $M = 1.0$ .

Changes in spanwise camber without changes in incidence distribution, do not alter the force characteristics near the design lift, but do alter the off-design characteristics.

UNCLASSIFIED

UNCLASSIFIED

subsonic speeds the cambered wings were less stable than the uncambered wing; also the changes of stability with incidence and Mach number were greater, particularly near  $M = 1.0$ .

Changes in spanwise camber without changes in incidence distribution, do not alter the force characteristics near the design lift, but do alter the off-design characteristics.

UNCLASSIFIED

UNCLASSIFIED



*Information Centre  
Knowledge Services*  
**[dstl]** Porton Down  
Salisbury  
Wiltshire  
SP4 0JQ  
22060-6218  
Tel: 01980-613753  
Fax 01980-613970

Defense Technical Information Center (DTIC)  
8725 John J. Kingman Road, Suit 0944  
Fort Belvoir, VA 22060-6218  
U.S.A.

AD#: AD 280149

Date of Search: 10 December 2008

Record Summary: DSIR 23/29561

Title: Further experimental investigations of the characteristics of cambered gothic wings at  
Mach numbers from 0.4 to 2.0 (RAE TN Aero 2803)  
Availability Open Document, Open Description, Normal Closure before FOI Act: 30 years  
Former reference (Department) ARC 23724  
Held by The National Archives, Kew

This document is now available at the National Archives, Kew, Surrey, United Kingdom.

DTIC has checked the National Archives Catalogue website  
(<http://www.nationalarchives.gov.uk>) and found the document is available and  
releasable to the public.

Access to UK public records is governed by statute, namely the Public  
Records Act, 1958, and the Public Records Act, 1967.

The document has been released under the 30 year rule.

(The vast majority of records selected for permanent preservation are made  
available to the public when they are 30 years old. This is commonly referred  
to as the 30 year rule and was established by the Public Records Act of  
1967).

This document may be treated as UNLIMITED.